NASA Contractor Report 159219

NASA-CR-159219
1980 0010155

STRESS INTENSITY FACTORS IN TWO BONDED ELASTIC LAYERS CONTAINING CRACKS PERPENDICULAR TO AND ON THE INTERFACE - PART II. SOLUTION AND RESULTS

Ming-Che Lu and F. Erdogan

LEHIGH UNIVERSITY
Bethlehem, Pennsylvania 18015

NASA Grant NGR 39-007-011
January 1980

National Aeronautics and
Space Administration

Langley Research Center
Hampton, Virginia 23665

STRESS INTENSITY FACTORS IN TWO BONDED ELASTIC LAYERS CONTAINING CRACKS PERPENDICULAR TO AND ON THE INTERFACE - PART II. SOLUTION AND RESULTS (*)

by

Ming-Che Lu and F. Erdogan
Lehigh University, Bethlehem, PA 18015

Abstract

The analysis of the title problem was given in Part I. In this part the numerical method for solving the problem is described and the stress intensity factors obtained from the solution for various crack geometries are presented.

1. Introduction

The formulation and analysis of the plane problem for two bonded infinite dissimilar elastic strips which contain cracks of various configurations is presented in Part I of this paper [1]. The problem is intended to approximate a composite beam or a plate having cracks perpendicular to and on the interface of the two layers. The crack geometries and some of their limiting cases which have been considered in the analysis are shown in Figure 1. This part of the paper is devoted to the solution of the problem for various typical crack geometries and to the presentation and discussion of the results.

(*) This work was supported by NSF under the Grant ENG 78-09737 and by NASA-Langley under the Grant NGR 39-007-011.

2. The Solution

In Part I the problem was shown to reduce to a system of four singular integral equations for the unknown functions $\phi_1,..,\phi_4$ which are defined by

$$\frac{\partial}{\partial x_i} v_i(x_i,+0) = \phi_i(x_i) \ , \ (i=1,2) \tag{1}$$

$$\frac{\partial}{\partial y}[v_1(+0,y) - v_2(2h_2-0,y)] = \phi_3(y) \ , \tag{2}$$

$$\frac{\partial}{\partial y}[u_1(+0,y) - u_2(2h_2-0,y)] = \phi_4(y) \ , \tag{3}$$

where u_i and v_i, $(i=1,2)$ are respectively the x and the y component of the displacement vector in the strips 1 and 2, and the general notation is shown in Figure 2. The system of singular integral equations are given by (19)-(21) of Part I. The integral equations are solved by using a Gauss-Chebyshev or a Gauss-Jacobi integration formula whenever possible, and a combination of a Gauss-Jacobi integration formula and the method of Jacobi series if the simple Gaussian integration methods are not applicable. In order to apply these techniques it is necessary to normalize the supports of the integral equations (19)-(21). These equations are of the following general form (see Figure 2):

$$\sum_{j=1}^{4} \int_{a_j}^{b_j} h_{ij}(x_i,s)\phi_j(s)\,ds = M_i p_i(x_i), \ i=1,2, \ a_i \le x_i \le b_i \ , \tag{4}$$

$$\sum_{j=1}^{4} \left[\int_{a_j}^{b_j} h_{ij}(y,s)\phi_j(s)\,ds + \gamma\,\delta_{ij}\,\phi_j(y) \right] = M_i p_i(y) \ , \quad i=3,4 \ , \ a_i < y < b_i \tag{5}$$

where $a_4 = a_3$, $b_4 = b_3$, the constant γ is given by (22)

of Part I, $p_1,..,p_4$ refer to the crack surface tractions and $M_1,..,M_4$ are material constants (see equations 9-11 of Part I). In the case of imbedded cracks the kernels h_{11}, h_{22}, h_{34}, h_{43} have a Cauchy-type singularity and the remaining kernels are bounded. For cracks intersecting the boundaries or each other all related kernels have generalized Cauchy-type singularities.

For the purpose of numerical solution the following normalized quantities are introduced:

$$t = \frac{2s}{b_j-a_j} - \frac{b_j+a_j}{b_j-a_j}, \quad (a_j<s<b_j, \ -1<t<1, \ j=1,..,4), \tag{6}$$

$$r = \frac{2x_i}{b_i-a_i} - \frac{b_i+a_i}{b_i-a_i}, \quad (a_i<x_i<b_i, \ -1<r<1, \ i=1,2), \tag{7}$$

$$r = \frac{2y}{b_3-a_3} - \frac{b_3+a_3}{b_3-a_3}, \quad (a_3<y<b_3, \ -1<r<1), \tag{8}$$

$$f_j(t) = \phi_j(s), \quad (j=1,..,4), \tag{9}$$

$$h_{ij}(x_i,s) = H_{ij}(r,t), \quad (a_i<x_i<b_i, \ a_j<s<b_j, \ -1<(r,t)<1, \ i=1,2; \ j=1,..,4), \tag{10}$$

$$h_{ij}(y,s) = H_{ij}(r,t), \quad (a_3<y<b_3, \ a_4=a_3, \ b_4=b_3, \ a_j<s<b_j, \ -1<(r,t)<1, \ i=3,4; \ j=1,..,4), \tag{11}$$

$$p_i(x_i) = P_i(r), \quad i=1,2, \ a_i<x_i<b_i, \ -1<r<1, \tag{12}$$

$$p_i(y) = P_i(r), \quad i=3,4, \ a_i<y<b_i, \ -1<r<1. \tag{13}$$

The system of integral equations (4) and (5) may then be expressed as

$$\sum_{j=1}^{4} \frac{b_j-a_j}{2} \int_{-1}^{1} H_{ij}(r,t)f_j(t)dt = M_iP_i(r), \quad i=1,2, \quad -1<r<1, \tag{14}$$

$$\sum_{j=1}^{4} \left[\frac{b_j-a_j}{2} \int_{-1}^{1} H_{ij}(r,t)f_j(t)dt + \gamma\delta_{ij}f_j(r)\right] = M_iP_i(r), \quad i=3,4 \ , \ -1<r<1. \tag{15}$$

Also, defining

$$f(r) = f_4(r)+i\ f_3(r), \quad P(r) = P_4(r)-i\ P_3(r), \tag{16a,b}$$

and combining the two integral equations given by (15) we obtain (see equations (20), (21), (26) and (27) of Part I)

$$\frac{1}{\pi i} \int_{-1}^{1} \frac{f(t)}{t-r}\, dt - \gamma\, f(r) + \int_{-1}^{1} \sum_{1}^{2} K_j(r,t)f_j(t)dt + \int_{-1}^{1} [K_3(r,t)f(t) + K_4(r,t)\bar{f}(t)]dt = M_3P(r), \quad -1<r<1, \tag{17}$$

where the kernels $K_1,..,K_4$ are complex functions.

Referring now to equations (24) and (28) of Part I and (9), (6) and (16a), the solution of the integral equations (14) and (17) may be expressed as follows:

$$f_j(t) = \frac{F_j(t)}{(1+t)^{\alpha_j}(1-t)^{\beta_j}} \ , \ 0<\mathrm{Re}(\alpha_j,\beta_j)<1, \ j=1,2, \tag{18}$$

$$f(t) = \frac{F(t)}{(1+t)^{\alpha_3}(1-t)^{\beta_3}} \ , \ 0<\mathrm{Re}(\alpha_3,\beta_3)<1 \ . \tag{19}$$

where for some typical crack geometries the characteristic equations to determine the constants α_j and β_j, (j=1,2,3) are given in Part I. For example, for the imbedded cracks we have

$$\alpha_1 = \beta_1 = \alpha_2 = \beta_2 = 1/2,\ \alpha_3 = \frac{1}{2} - i\omega,\ \beta_3 = \frac{1}{2} + i\omega,$$

$$\omega = \frac{1}{2\pi} \log \left(\frac{1+\gamma}{1-\gamma}\right) . \qquad (20)$$

Note that the integral equations (14) are of the first kind and the constants α_j and β_j, (j=1,2) are always real. Consequently, the related Chebyshev polynomials $T_n(t)$ (corresponding to $\alpha_j = 0.5 = \beta_j$) or Jacobi polynomials $P_n^{(-\beta_j,-\alpha_j)}(t)$ have n real roots t_k, $-1<t_k<1$. Therefore, in this case a Gaussian integration formula can be developed to evaluate the singular integrals and the integral equations may be replaced by a system of algebraic equations for the unknowns $F_j(t_k)$, j=1,2, $T_n(t_k)=0$, (or $P_n^{(-\beta_j,-\alpha_j)}(t_k) = 0$), k=1,..,n (see, for example [2]). On the other hand (17) is a singular integral equation of the second kind having a dominant part with complex coefficients. Therefore, the constants α_3 and β_3 will always be complex and the roots of the related Jacobi polynomials $P_n^{(-\beta_j,-\alpha_3)}(t)$ will have complex roots. Since these roots are not on the line of integration $-1<t<1$, it is not possible to develop a Gaussian integration formula to evaluate the dominant part of the integral equations in terms of a discrete set of unknowns $F(t_k)$, k=1,..,n. A convenient method to solve this integral equation is the method of related orthogonal polynomials described in [3] (see also [2] and [4] for applications). Referring to (19) and observing that

$$w(t) = (1-t)^{\alpha}(1+t)^{\beta} ,\ (\alpha = -\beta_3,\ \beta = -\alpha_3), \qquad (21)$$

is the weight function of the Jacobi polynomials $P_n^{(\alpha,\beta)}(t)$,

in order to solve the integral equation the unknown function f(t) is expressed as

$$f(t) \cong \sum_{o}^{N} c_j P_j^{(\alpha,\beta)}(t)w(t) \ , \tag{22}$$

where $c_o,..,c_N$ are unknown complex coefficients. Using now the following property of the Jacobi polynomials

$$\frac{1}{\pi i}\int_{-1}^{1} P_j^{(\alpha,\beta)}(t)w(t)\frac{dt}{t-r} - \gamma\, P_j^{(\alpha,\beta)}(r)w(r)$$

$$= \frac{1}{2i}(1-\gamma^2)^{1/2}\, P_{j-1}^{(-\alpha,-\beta)}(r), \ -1<r<1, \tag{23}$$

the integral equation (17) may be written as

$$\sum_{j=0}^{N} \frac{1}{2i}(1-\gamma^2)^{1/2}\, c_j P_{j-1}^{(-\alpha,-\beta)}(r) + \int_{-1}^{1} \sum_{1}^{2} K_j(r,t)f_j(t)dt$$

$$\sum_{j=0}^{N} \int_{-1}^{1} [c_j K_3(r,t)P_j^{(\alpha,\beta)}(t)w(t)+\bar{c}_j K_4(r,t)\bar{P}_j^{(\alpha,\beta)}(t)\bar{w}(t)]dt$$

$$= M_3 P(r) \ , \ -1<r<1. \tag{24}$$

Using now the following Gaussian integration formula which corresponds to the weight functions defined by (18) [5]

$$\int_{-1}^{1} \frac{g(t)dt}{(1-t)^{\beta_j}(1+t)^{\alpha_j}} \cong \sum_{k=1}^{n} W_k g(t_k) \ , \tag{25}$$

after evaluating the integrals (24) may be expressed as

$$\sum_{j=0}^{N} \frac{1}{2i}(1-\gamma^2)^{1/2} c_j P_{j-1}^{(-\alpha,-\beta)}(r) + \sum_{m=1}^{2} \sum_{k=1}^{n} K_m(r,t_k)W_k F_m(t_k)$$

$$+ \sum_{j=0}^{N} [c_j Q_{3j}(r) + \bar{c}_j Q_{4j}(r)] = M_3 P(r), \ -1<r<1. \tag{26}$$

Note that

$$w(t) = (1+t)^{-\alpha_3}(1-t)^{-\beta_3} = \left(\frac{1+t}{1-t}\right)^{i\omega}(1-t^2)^{-1/2} . \qquad (27)$$

Hence the functions Q_{3j} and Q_{4j} may be evaluated quite simply by using the following Gaussian integration formula [5]

$$\int_{-1}^{1} p(t)(1-t^2)^{-1/2}dt = \sum_{1}^{n} \frac{\pi}{n} p(t_k), \quad t_k = \cos\frac{\pi(2k-1)}{2n} . \qquad (28)$$

In order to reduce (26) to a system of algebraic equations for the unknown constants c_j and $F_m(t_k)$ one may use a simple weighted residual method. In this case, it is clear that the related orthogonal polynomials are the Jacobi polynomials $P_n^{(-\alpha,-\beta)}(t)$, n=0,1,... . Thus, using the orthogonality relation

$$\int_{-1}^{1} P_n^{(\alpha,\beta)}(t)P_m^{(\alpha,\beta)}(t)w(t)dt = \begin{cases} 0 , & n \neq m \\ \theta_n(\alpha,\beta), & n=m , \end{cases} \qquad (29)$$

$$\theta_n(\alpha,\beta) = \frac{2^{\alpha+\beta+1}\Gamma(n+\alpha+1)\Gamma(n+\beta+1)}{(2n+\alpha+\beta+1)(n+\alpha+\beta+1)n!} ,$$

multiplying both sides of (26) by

$$(1-r)^{-\alpha}(1+r)^{-\beta}P_\ell^{(-\alpha,-\beta)}(r), \quad \ell = 0,1,..,N-1$$

and integrating in (-1,1) we find

$$\frac{1}{2i}(1-\gamma^2)^{1/2}c_{\ell+1}\,\theta_\ell(-\alpha,-\beta) + \sum_{m=1}^{2}\sum_{k=1}^{n} a_{\ell mk}F_m(t_k)$$

$$+ \sum_{j=0}^{N}[b_{\ell j}c_j + d_{\ell j}\bar{c}_j] = A_\ell , \quad (\ell=0,1,..,N-1). \qquad (30)$$

Again, the constants a, b, and d may be evaluated by using the Gaussian integration formula (28).

Similarly, the integral equations (14) may easily be reduced to a system of algebraic equations in $F_m(t_k)$ and c_j. The first two terms in (14) may be expressed in terms of $F_m(t_k)$ by using the integration formula (25) and (18) [2] giving

$$\int_{-1}^{1} H_{ij}(r_s,t)f_j(t)dt \cong \sum_{k=1}^{n} W_k H_{ij}(r_s,t_k)F_j(t_k) ,$$

$$i=1,2,\ j=1,2,\ s=1,..,n-1 \qquad (31)$$

where t_k and r_s are the roots of the corresponding Chebyshev or Jacobi polynomials. The last two terms on the left hand side of (14) which contains f_3 and f_4 involve real and imaginary parts of the integrals

$$\int_{-1}^{1} H_{ij}(r_s,t)P_{\ell}^{(\alpha,\beta)}(t)w(t)dt,$$

which may easily be evaluated by using the integration formula (28).

It should be observed that by using the procedure outlined above the integral equations (14) and (17) have been reduced to 2n-2+2N real algebraic equations in 2n+2N+2 real unknowns $F_m(t_k)$, (m=1,2; k=1,..,n) and the real and imaginary parts of c_j, (j=0,..,N). The remaining four equations are provided by four additional conditions corresponding to the single-valuedness of displacements, the requirement of boundedness of the displacement derivatives, and the relations between the displacement derivatives for intersecting cracks (see Part I). For example, for an imbedded crack $0<a_1<b_1<2h_1$ (see Figure 2)

$$\int_{a_1}^{b_1} \phi_1(s)ds=0, \text{ or } \sum_{1}^{n} \frac{\pi}{n} F_1(t_k) = 0 , \qquad (32)$$

and for an edge crack $0<a_1<b_1 = 2h_1$, $F_1(1) = 0$, etc.(*) The details of the numerical solution for each typical crack geometry may be found in [6].

From the definitions given by (1), (2), (3), and (9) it is seen that once the functions $f_1,..,f_4$ are determined, one may obtain the desired crack surface displacements by means of routine integrations.

3. Stress Intensity Factors

The stress intensity factors were defined in Section 5 of Part I. In Part I it was also shown that the stress intensity factors may be calculated directly from the asymptotic expansion of the displacement derivatives $\phi_1,..,\phi_4$ around the crack tips. Thus, aside from a multiplying factor, the constants $F_j(\mp 1)$, $(j=1,..,4)$ give the stress intensity factors. For example, from equation (62a) of Part I and (6), (9) and (18) it follows that for an imbedded crack $0<a_2<b_2<2h_2$ the stress intensity factors may be expressed as

$$k(a_2) = \frac{4\mu_2}{1+\kappa_2} F_2(-1) \sqrt{(b_2-a_2)/2} ,$$

$$k(b_2) = - \frac{4\mu_2}{1+\kappa_2} F_2(1) \sqrt{(b_2-a_2)/2} . \qquad (33a,b)$$

Similar expressions can be obtained for all other crack geometries.

4. Results and Discussion

The particular crack configurations for which the problem is solved numerically are shown in Figure 1. The results are given in Figures 3-36. With the exception

---

(*) In this case $f_1(+1)$ has the indefinite form 0/0 and, if needed, may be evaluated as a limit.

of a few crack geometries for which crack surface displacements are calculated, the results given in this paper refer to the stress intensity factors. Generally the results presented in the figures are self-explanatory. Hence a detailed discussion of each figure does not seem to be necessary.

The results given in this paper are obtained for self-equilibrating crack surface tractions. If the external loads are applied to the layered material at locations sufficiently far from the region of cracks, then the crack surface tractions in the perturbation problem would be uniform. For example, if the medium is loaded in tension parallel to the y-axis away from the crack region the crack surface tractions are constant and are related by

$$\frac{(1-\nu_1^2)p_1}{E_1} = \frac{(1-\nu_2^2)p_2}{E_2}\ ,\ p_3 = 0,\ p_4 = 0 \qquad (34)$$

for plane strain and

$$\frac{p_1}{E_1} = \frac{p_2}{E_2}\ ,\ p_3 = 0,\ p_4 = 0 \qquad (35)$$

for plane stress. In this paper only plane strain case is considered.

Figure 3 shows the stress intensity factors for a simple imbedded crack of length $2\ell_2 = h_2$. Note that as the crack tip b_2 approaches the interface (i.e., as $c \to \ell_2$) $k(b_2)$ tends to zero for $\mu_2 < \mu_1$ and to infinity for $\mu_2 > \mu_1$. This well-known behavior is due to the fact that for $b_2 = 2h_2$ the power of the stress singularity β_2 is greater than 0.5 if $\mu_2 > \mu_1$ and less than 0.5 if $\mu_2 < \mu_1$ [see, for example [7]]. For this case the definition of the stress intensity factor and the behavior of the stress state around the crack tip are given by the equations (65) and (67) of Part I. For the material combinations used in Figure 3

$\beta_2 = 0.624348$ for $\mu_2>\mu_1$ and $\beta_2 = 0.385339$ for $\mu_2<\mu_1$. Also note that as the crack tip a_2 approaches the free boundary as expected, $k(a_2)$ tends to infinity.

Stress intensity factors for an edge crack are shown in Figures 4 and 5. In this case too note that as the crack tip b_2 approaches the interface $k(b_2)$ tends to zero for $\mu_2<\mu_1$ and to infinity for $\mu_2>\mu_1$. Also note that as the crack length decreases the stress intensity factor ratio approaches 1.586 which is the value obtained for the semi-infinite plane having an edge crack of length $2\ell_2$. Figure 6 shows the effect of stiffness ratio for a fixed crack geometry. Note that as $\mu_1/\mu_2 \to 0$ the stress intensity factors approach the value for an edge-cracked strip under uniform tension $k(b_2) \tilde{=} 3.99\ p_2\sqrt{\ell_2}$. The effect of thickness ratio is shown in Figures 7 and 8. The results for the crack terminating at the interface are shown in Figures 9-11 as well as in Figures 7 and 8 (the curves corresponding to $\ell_2/h_2=1$).

Figures 10 and 11 show the stress intensity factors in a layered plate containing an edge crack and subjected to uniform bending away from the crack region. In the uncracked composite plate the relevant stress is given by (see Figure 2 and insert in Figure 10)

$$\sigma_{2yy}(x_2,0) = -p_2(x_2) = -p_2(1-x_2/c_2) \qquad (36)$$

$$c_2 = [E_1(h_1^2+2h_1h_2)+E_2h_2^2]/(E_1h_1+E_2h_2) \qquad (37)$$

where $x_2=c_2$ determines the location of the neutral axis and the constant p_2 is the magnitude of the stress at the surface which is related to the bending moment M by

$$p_2 = \frac{3c_2M}{2(2h_1-c_1)^3+3c_1^3-c_2^3}\ ,\ c_1 = 2(h_1+h_2)-c_2\ . \qquad (38)$$

One may note that since the powers of stress singularity are different, the direct comparison of the stress intensity factors for the two cases shown in Figure 11 would be meaningless.

The stress intensity factors in bonded layers containing two (collinear) edge cracks and subjected to tensile loads away from the crack region are shown in Figures 12 and 13. Note that in this case the stress intensity factor in the layer with the smaller stiffness is generally smaller than that in the layer with greater stiffness, decreases with increasing crack length, and eventually becomes negative. This, of course, is due to the "bending" of the notched composite layer. In the figures the negative stress intensity factor is shown by dashed lines. If there are no other external loads to offset this effect through superposition, the results given in the figures for $k<0$ are not valid.

To give some idea about the effect of Poisson's ratios on the stress intensity factor in the case of a broken layer Figure 14 shows the results for varying ν_1 and fixed values of $\nu_2=0.3$ and $\mu_1=2\mu_2$. It is important to note that in this case the power of stress singularity $\beta_2=\alpha$ is also a function of ν_1, which is given in Table 1. Thus, even though the figure shows the stress intensity factor slightly increasing with ν_1, since α is a decreasing function of ν_1, the intensity of the stress state at the crack tip would actually decrease with ν_1 (see equations (65) and (67) of Part I).

Table 1. Power of stress singularity $\beta_2=\alpha$ for a crack terminating at the interface, $\nu_2=0.3$, $\mu_1=2\mu_2$.

ν_1	0	0.05	0.10	0.15	0.20	0.25
α	0.483251	0.476747	0.469679	0.461967	0.453516	0.444205

ν_1	0.30	0.35	0.40	0.45	0.50
α	0.433891	0.422389	0.409466	0.394818	0.378041

Stress intensity factors for a crack crossing the interface are given in Figures 15-19. The results for an imbedded crack are shown in Figures 15 and 16. Note that as the crack tip a_2 approaches the interface, due to again the change in the power of stress singularity, the stress intensity factors become unbounded. Also as $a_2 \to 0$, $k(a_2) \to \infty$. The results for the edge crack (i.e., for $a_2=0$) are given in Figures 17-19. As $h_1 \to 0.2\ h_2$, the crack tip b_1 approaches the free boundary and consequently $k(b_1) \to \infty$. Figures 18 and 19 show the stress intensity factors k_x and k_{xy} at the interface. It should be noted that even though the magnitudes of k_x and k_{xy} increase rapidly with decreasing net ligament thickness $2(h_1-0.2h_2)$, $h_1/h_2=0.2$ is not an asymptote of k_x and k_{xy}. Figure 20 shows some sample results for the crack surface displacement.

An important special case of the crack crossing the interface is the stress-free end problem for two bonded semi-infinite plates or beams. In this case the problem may be solved by letting $a_1=0=a_2$, $b_1=2h_1$ and $b_2=2h_2$ (see Figure 2) and properly treating the singular behavior of the solution at the irregular points $x_2=0$, $x_2=2h_2$, $x_1=0$, and $x_1=2h_1$ (see Part I). The problem may be one of thermal stress, residual stress, or mechanical loading. The technique for isolating the perturbation problem in which self-equilibrating end tractions are the only external loads is relatively straightforward. Invariably one imagines an infinite plate ($-\infty<y<\infty$, $-\infty<z\infty$, $0<x_1<2h_1$, $0<x_2<2h_2$) under a given set of applied loads and calculates the stresses at y=0 plane. The needed tractions in the perturbation problem are the equal and opposite of these stresses. For example if a clamped plate is pulled in z-direction or heated uniformly, the perturbation problem would have to be solved under a system of self-equilibrating tractions on the boundary y=0 which consists of constant normal stresses p_1 and p_2 and the linearly distributed

stress coming from a bending moment M which are related by

$$p_1 h_1 + p_2 h_2 = 0, \quad M = 2p_1 h_1 (h_1+h_2). \tag{39}$$

The stresses resulting from M would be obtained from equations such as (36)-(38). Figure 21 shows the results of such an example.

In the stress-free end problem, after solving the integral equations and obtaining the density functions ϕ_1 and ϕ_2 the relative displacements in y-direction on the boundary y=0 may easily be evaluated (see equation (1)) from

$$v_1(x_1,0) = v_o + \int_0^{x_1} \phi_1(s)ds,$$

$$v_2(x_2,0) = v_o - \int_{x_2}^{2h_2} \phi_2(s)ds, \tag{40a,b}$$

where $v_o = v_1(0,0) = v_2(0,0)$ represents a rigid body motion. Figure 22 shows some sample results for the displacements.

The results for a uniformly pressurized T-shaped crack are shown in Figures 23-25. Note that due to pressure p_3 for small values of the crack length $2\ell_2$ the stress intensity factor $k(a_2)$ becomes negative (Figure 24).

Figures 26-29 show the results for bonded layers containing a T-shaped crack and loaded in y-direction away from the crack region for which $p_3=p_4=0$ and p_2 is constant.

The results for a symmetric cross-shaped crack are given in Figures 30 and 31. The external load in this example is the tension in y-direction away from the crack region. Corresponding results for $a_2=0$, i.e., for a broken layer are shown in Figures 32-34. The crack surface pressures used in the example given in Figures 32 and 33 correspond to uniform tension in x direction as well as

tension in y direction away from the crack region. The results for tension in y direction only are given in Figure 34.

The results for an edge crack in a bonded semi-infinite plate are shown in Figures 35 and 36. The extermal load in these examples correspond to a uniform tension in z-direction or uniform heating or cooling of a clamped plate. Note that for this crack configuration the dominant stress intensity factor is the shear component k_2. From Figure 36 one may also observe that for bonded plates with equal thicknesses the magnitudes of the stress intensity factors are rather small.

Finally, it should be pointed out that the accuracy of the numerical results given in this paper is not uniform. For Mode I stress intensity factors at an imbedded crack tip it was possible to obtain a two-digit accuracy without any difficulty. However, in the calculation of the stress intensity factors at the interface crack tips and at the intersection of the crack and the interface there were convergence difficulties.

References:

1. Ming-Che Lu and F. Erdogan, "Stress Intensity Factors in Two Bonded Elastic Layers Containing Cracks Perpendicular To and On The Interface", Part I. Analysis. NASA CR-159218, 1980.
2. F. Erdogan, "Mixed Boundary Value Problems in Mechanics", Mechanics Today, Vol. 4, S. Nemat-Nasser, ed.,Pergamon Press, Oxford, pp. 1-85, 1978.
3. F. Erdogan, "Approximate Solution of Systems of Singular Integral Equations", SIAM J. on Appl. Math., Vol. 17, pp. 1041-1059, 1969.
4. F. Erdogan and G.D. Gupta, "On The Numerical Solution of Singular Integral Equations", Quarterly of Applied Mathematics, pp. 525-534, 1972.
5. M. Abramowitz and I.A. Stegun, Handbook of Mathematical Functions, N.B.S. Applied Mathematics Series 55, 1964.

6. Ming-Che Lu, "A Composite of Two Bonded Strips Containing Perpendicular Cracks and an Interface Crack", Ph.D. Dissertation, Lehigh University, 1978.

7. T.S. Cook and F. Erdogan, "Stresses in Bonded Materials with a Crack Perpendicular to the Interface", Int. J. Engng. Sci., Vol. 10, pp. 667-697, 1972.

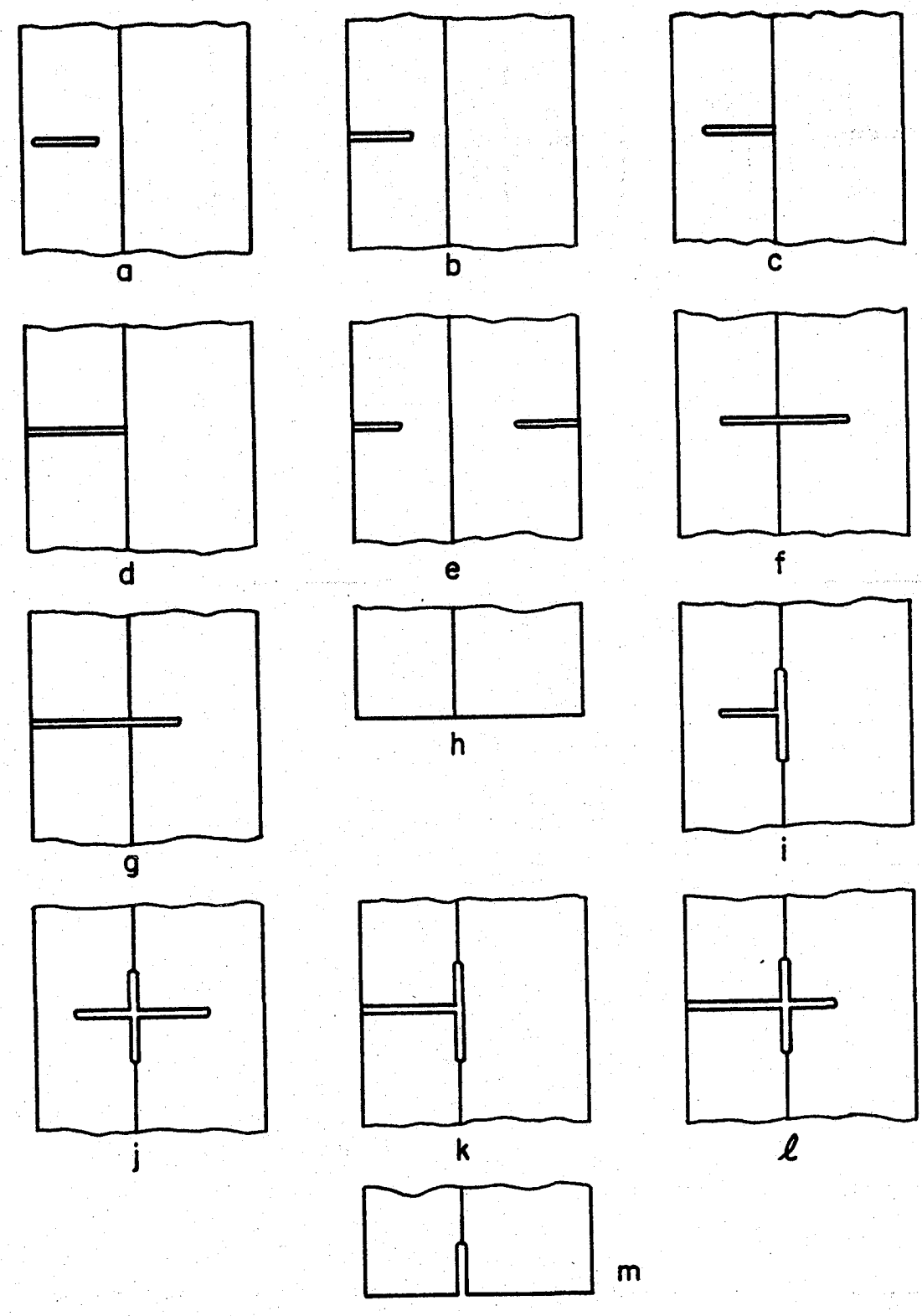

Figure 1. Crack configurations considered in the paper.

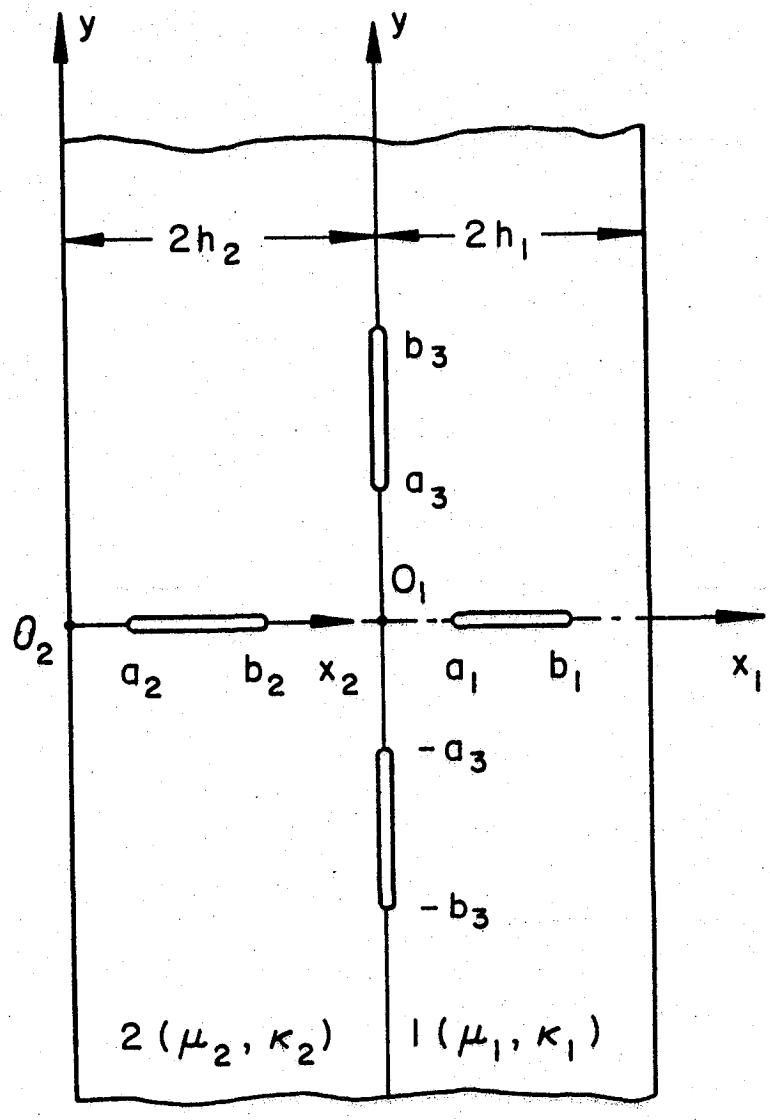

Figure 2. Geometry and notation of the crack problem.

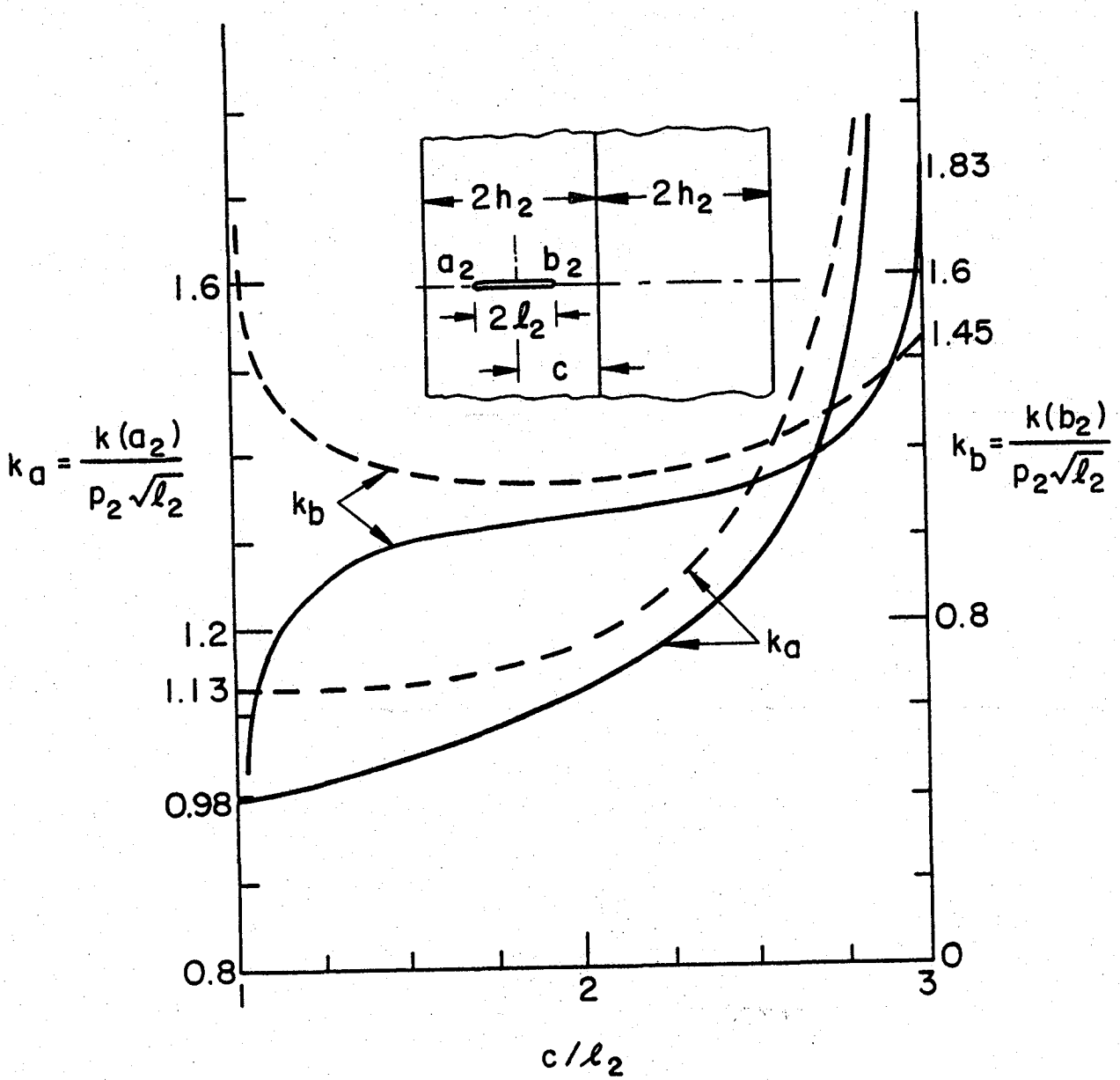

Figure 3. Stress intensity factors in two bonded layers containing a single crack under constant pressure p_2. $2\ell_2 = b_2 - a_2 = h_2$; solid lines: $\mu_1 = 3\mu_2$, $\nu_1 = 0.3$, $\nu_2 = 0.25$; dashed lines: $\mu_1 = \mu_2/3$, $\nu_1 = 0.25$, $\nu_2 = 0.3$. $k(a_2) = \lim_{x_2 \to a_2} \sqrt{2(a_2 - x_2)}\,\sigma_{2yy}(x_2, 0)$, $k(b_2) = \lim_{x_2 \to b_2} \sqrt{2(x_2 - b_2)}\,\sigma_{2yy}(x_2, 0)$.

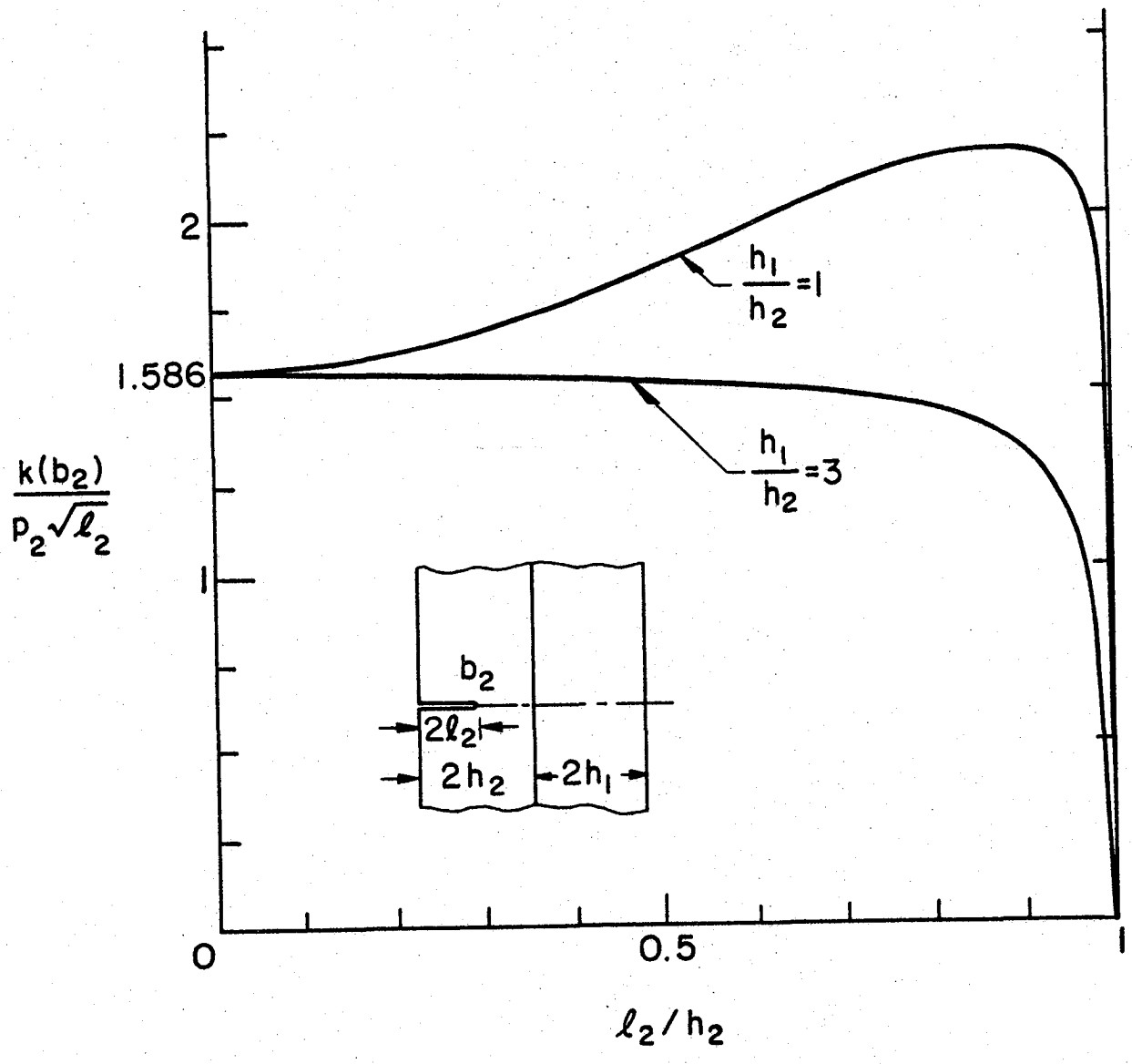

Figure 4. Stress intensity factor in two bonded layers with a pressurized edge crack $\mu_1=3\mu_2$, $\nu_1=\nu_2=0.3$.

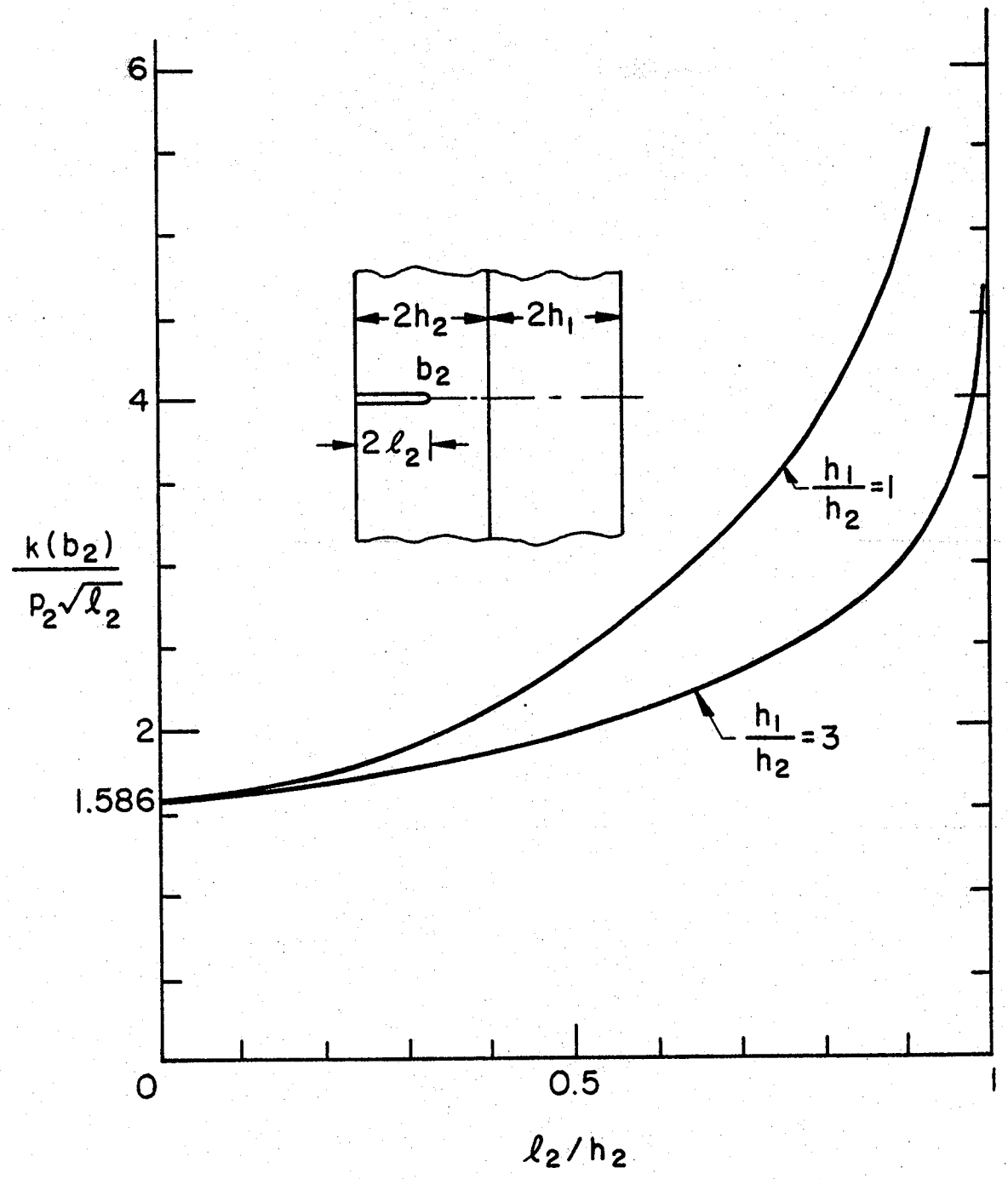

Figure 5. Stress intensity factor in bonded layers with a pressurized edge crack. $\mu_1=\mu_2/3$, $\nu_1=\nu_2=0.3$.

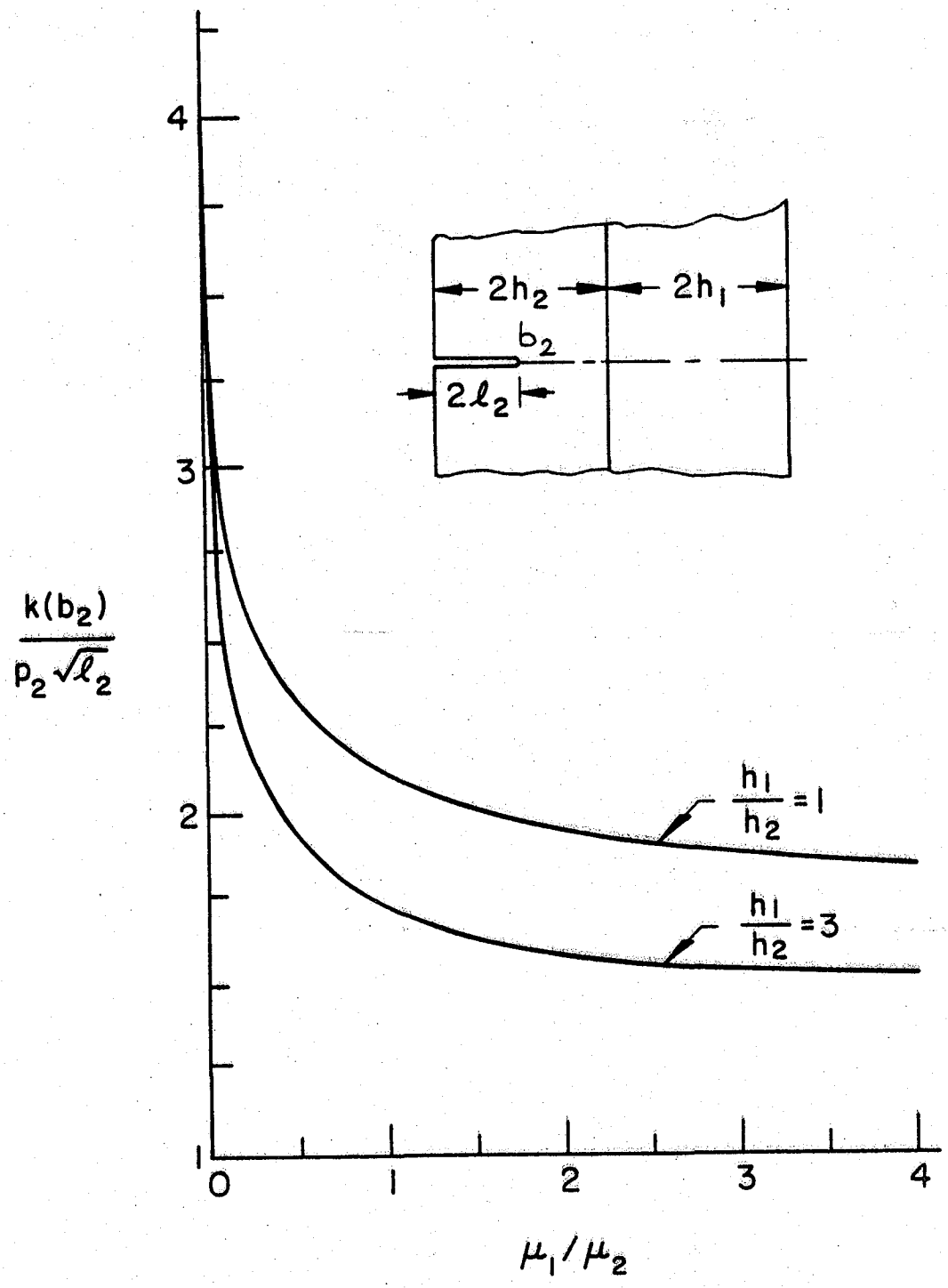

Figure 6. The effect of the stiffness ratio μ_1/μ_2 on the stress intensity factor in bonded layers with a pressurized edge crack. $\nu_1=\nu_2=0.3$, $2\ell_2=b_2=h_2$.

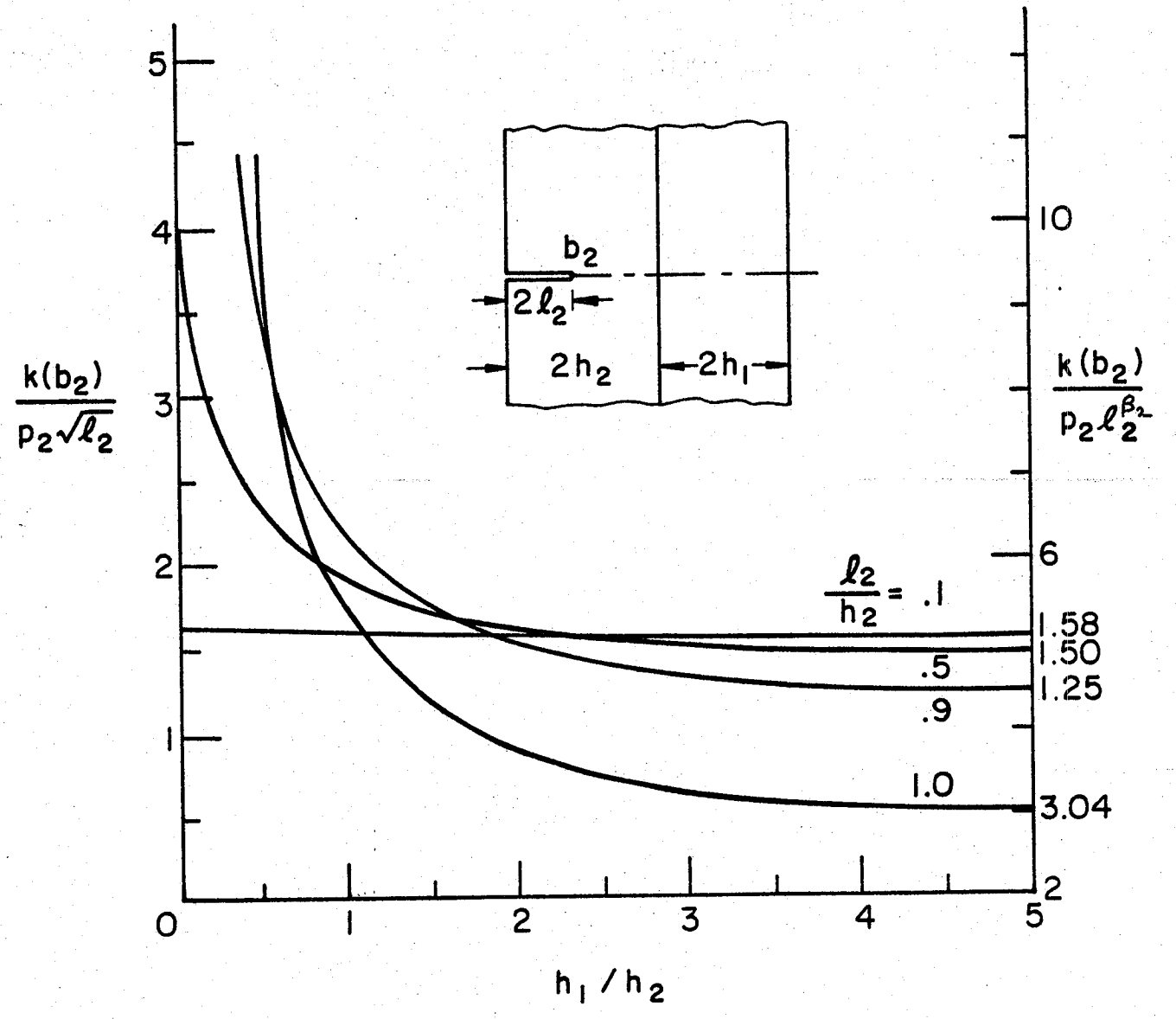

Figure 7. The effect of thickness ratio on the stress intensity factor in bonded layers with a pressurized edge crack. $\mu_1=3\mu_2$, $\nu_1=0.3$, $\nu_2=0.25$, $\beta_2=0.385339$ (for the crack touching the interface: $\ell_2=h_2$). $\ell_2<h_2$: $k(b_2)=\lim_{x_2\to b_2}\sqrt{2(x_2-b_2)}\sigma_{2yy}(x_2,0)$, $\ell_2=h_2$: $k(b_2)=\lim_{x_1\to 0}\sqrt{2}\, x_1^{\beta_2}\sigma_{1yy}(x_1,0)$.

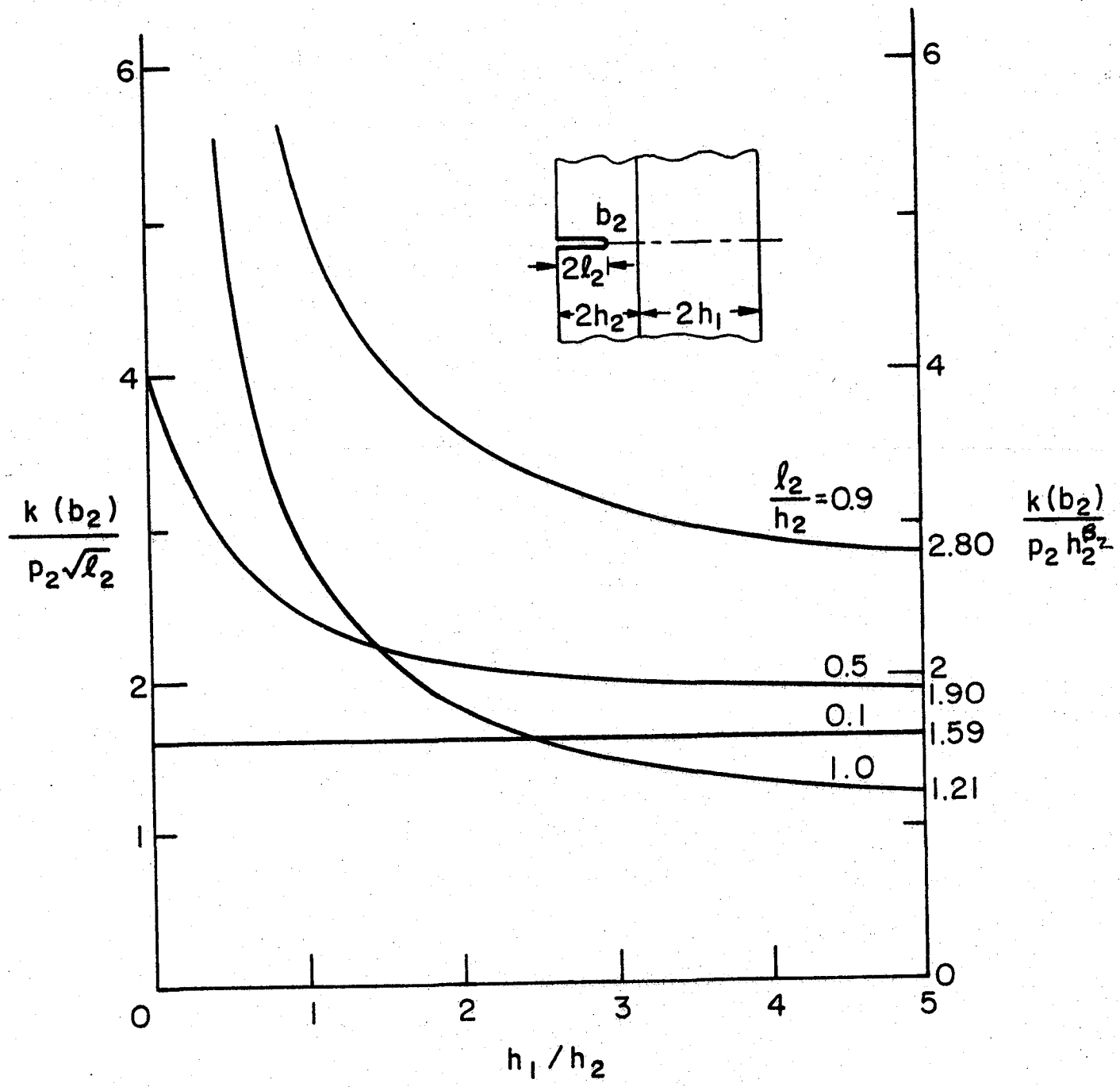

Figure 8. Same as Figure 7. $\mu_1=\mu_2/3$, $\nu_1=0.25$, $\nu_2=0.3$, $\beta_2=0.624348$ (for $\ell_2=h_2$).

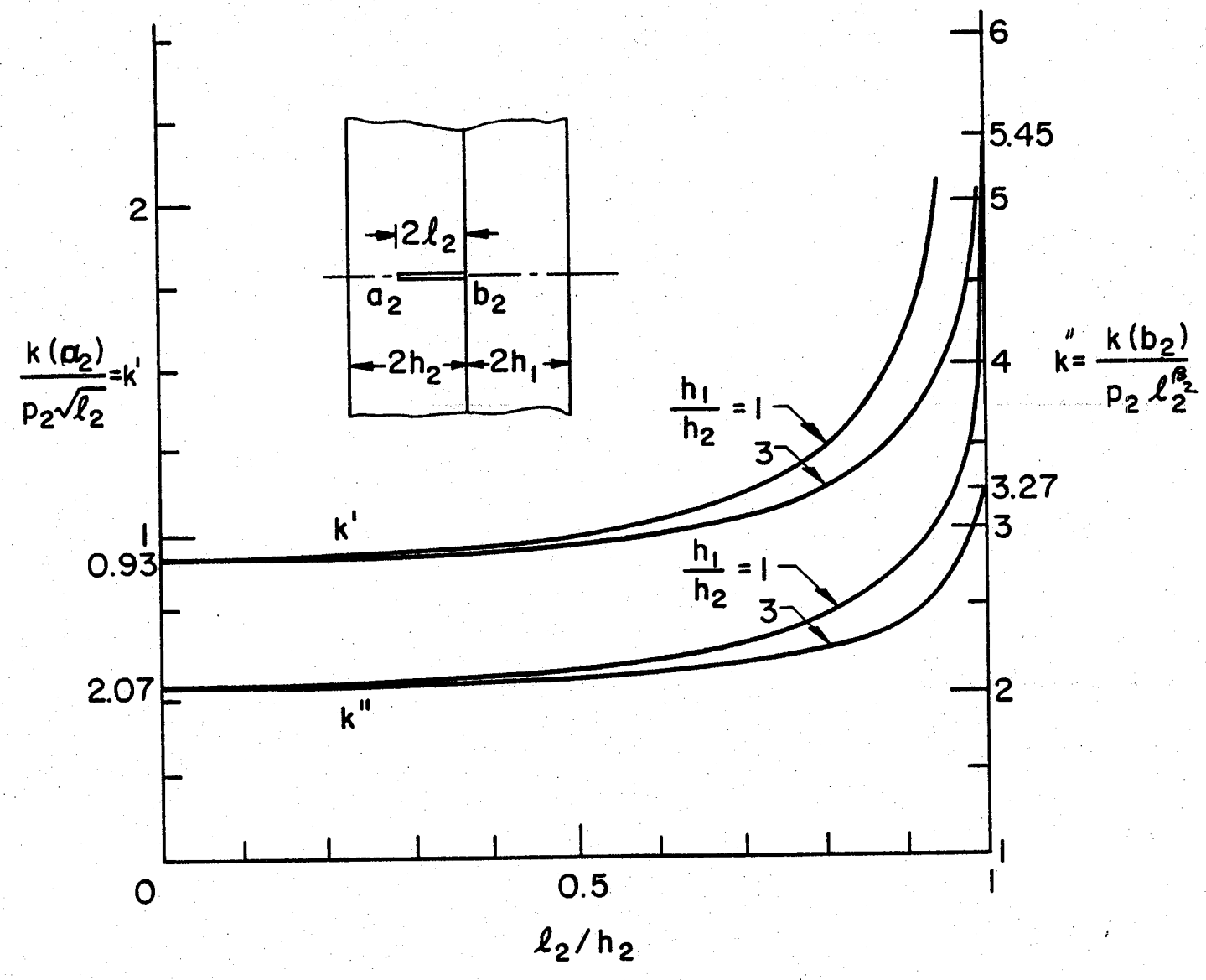

Figure 9. Stress intensity factors for an imbedded crack touching the interface. $\mu_1=3\mu_2$, $\nu_1=0.25$, $\nu_2=0.3$, external load: uniform crack surface pressure. $k(a_2)=\lim_{x_2\to a_2}\sqrt{2(a_2-x_2)}\sigma_{2yy}(x_2,0)$, $k(b_2)=\lim_{x_1\to 0}\sqrt{2}x_1^{\beta_2}\sigma_{1yy}(x_1,0)$.

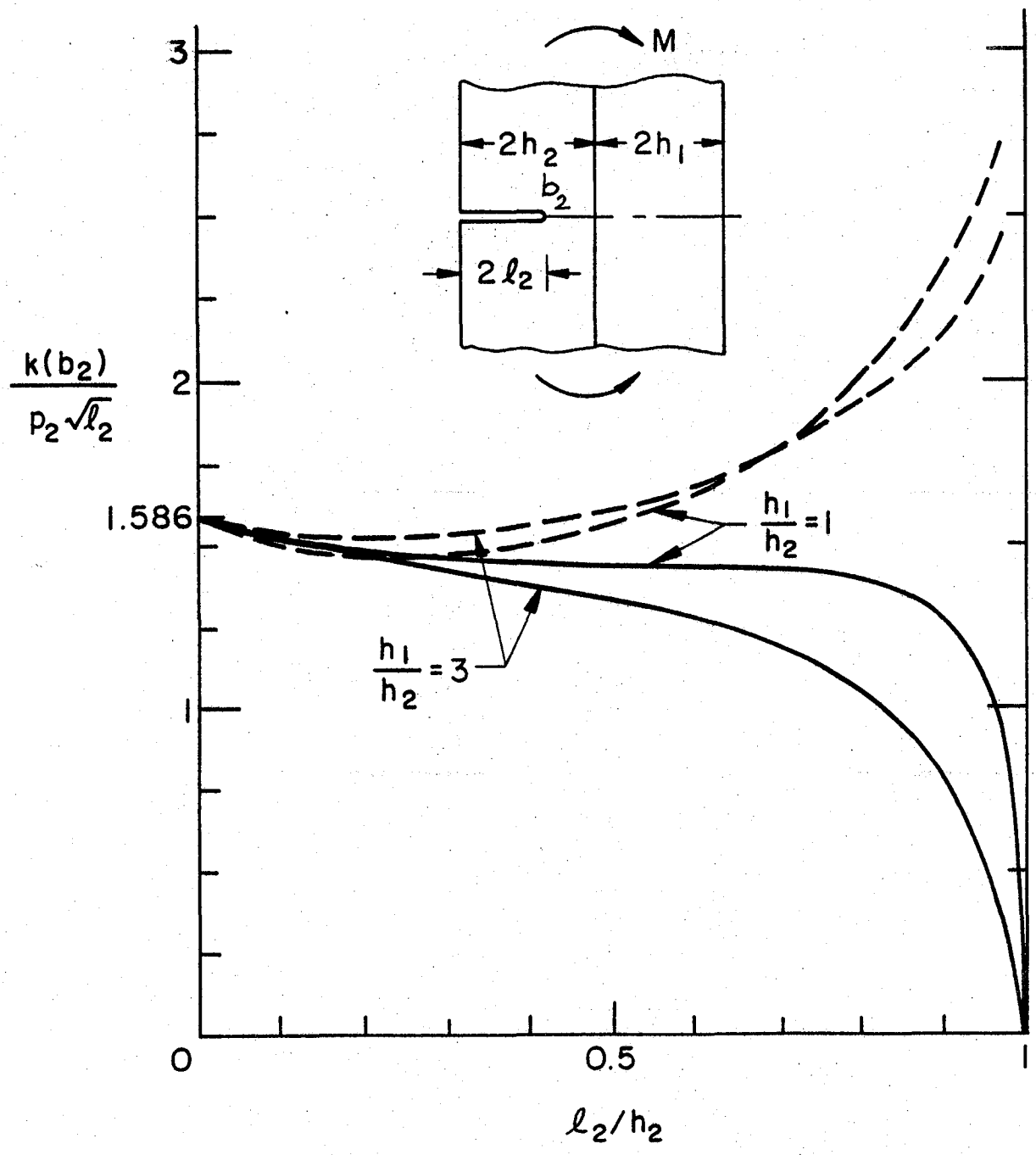

Figure 10. Stress intensity factor in bonded layers containing an edge crack and subjected to uniform bending away from the crack region. $\nu_1=\nu_2=0.3$, solid lines: $\mu_1=3\mu_2$, dashed lines: $\mu_1=\mu_2/3$. $k(b_2)=\lim_{x_2\to b_2}\sqrt{2(x_2-b_2)}\sigma_{2yy}(x_2,0)$.

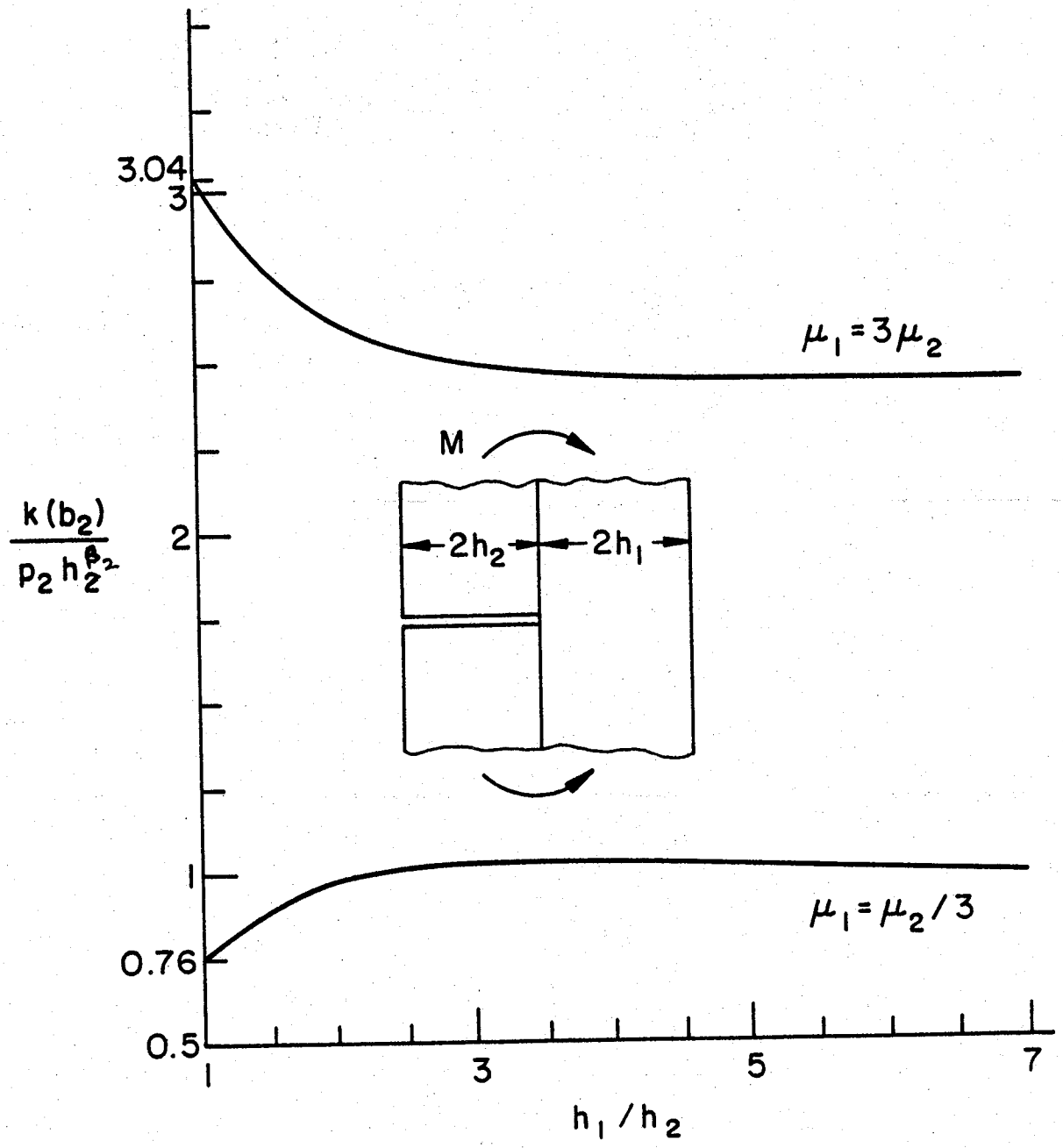

Figure 11. Stress intensity factor in the composite plate with a broken layer subjected to uniform bending. $\nu_1=\nu_2=0.3$. Power of stress singularity $\beta_2=0.400470$ for $\mu_1=3\mu_2$ and $\beta_2=0.620492$ for $\mu_1=\mu_2/3$. $k(b_2)=\lim_{x_1\to 0} \sqrt{2}\, x_1^{\beta_2}\, \sigma_{1yy}(x_1,0)$.

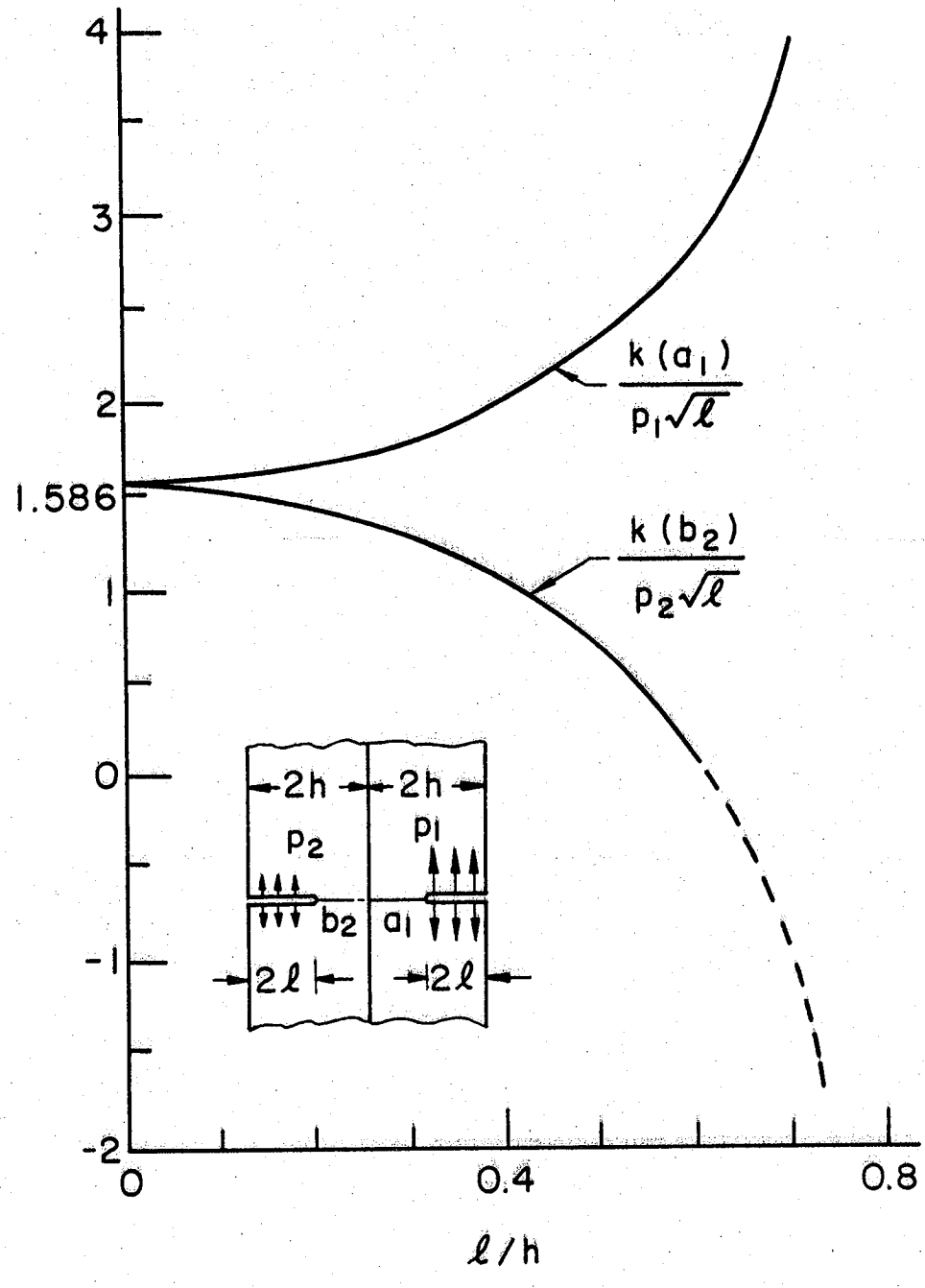

Figure 12. Stress intensity factors in bonded layers with double edge cracks. $\mu_1=3\mu_2$, $\nu_1=\nu_2=0.3$, external loads: uniform crack surface pressures, $p_1=3p_2$, $h_1=h_2=h$, $2\ell_1=2\ell_2=2\ell$. $k(a_1) = \lim_{x_1\to a_1} \sqrt{2(a_1-x_1)}\sigma_{1yy}(x_1,0)$, $k(b_2)=\lim_{x_2\to b_2}\sqrt{2(x_2-b_2)}\sigma_{2yy}(x_2,0)$.

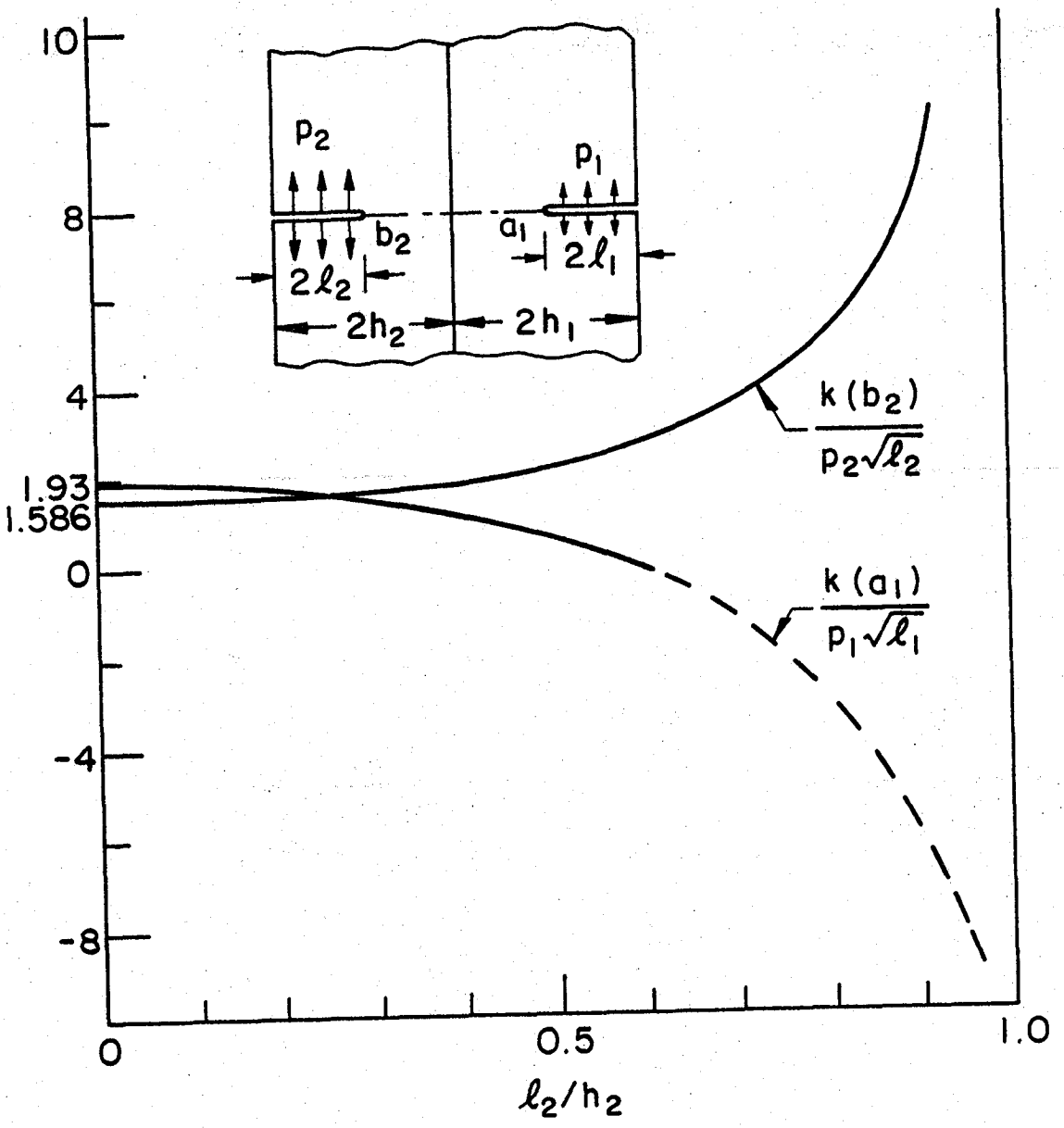

Figure 13. Stress intensity factors for double edge cracks. $\mu_1=\mu_2/3$, $\nu_1=\nu_2=0.3$, $h_1=h_2$, $2\ell_1=h_1$, $p_1=p_2/3$.

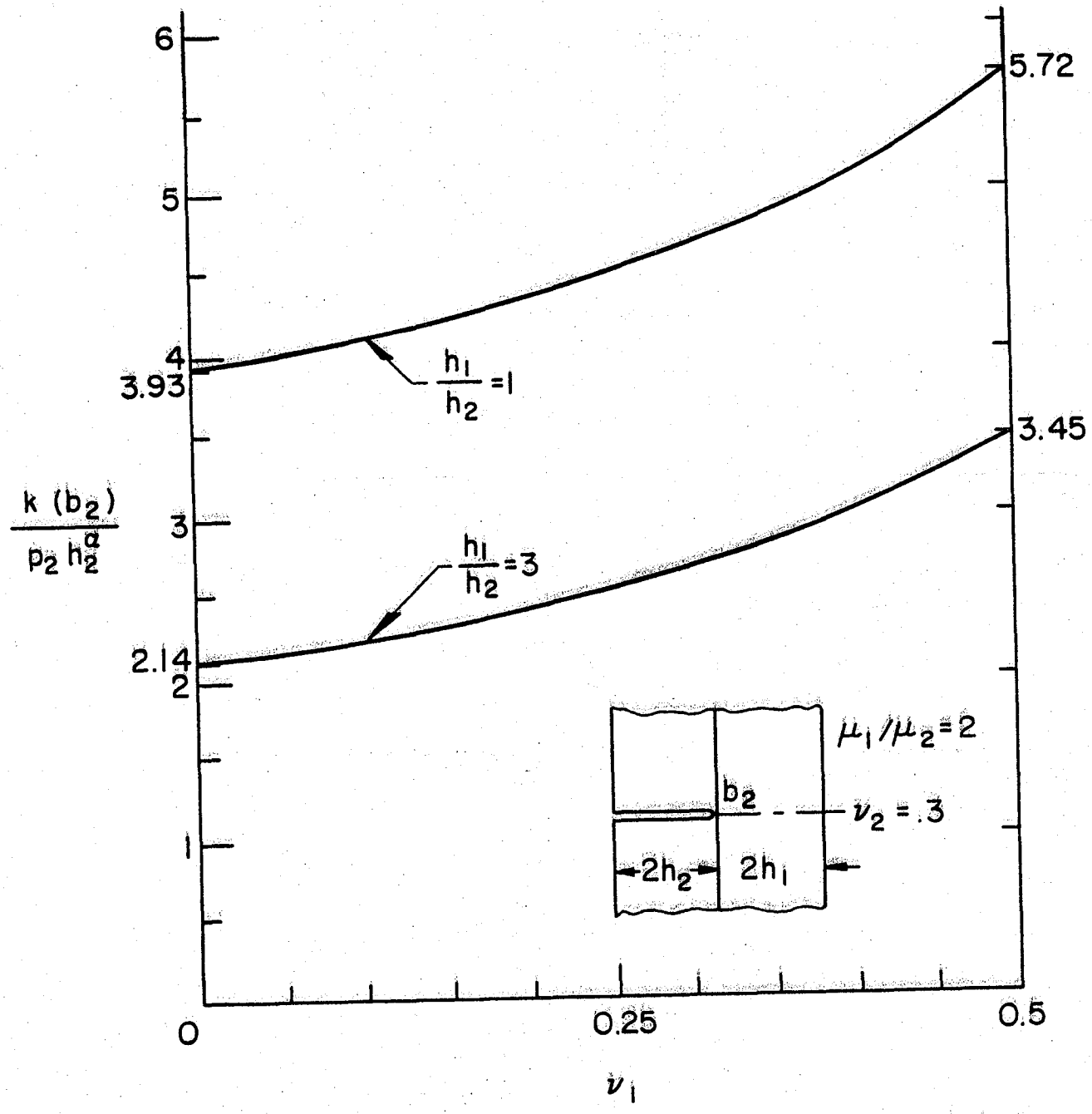

Figure 14. Effect of Poisson's ratio on the stress intensity factors in bonded layers with an edge crack touching the interface (note: α is also dependent on ν_1 and is given in Table 1).

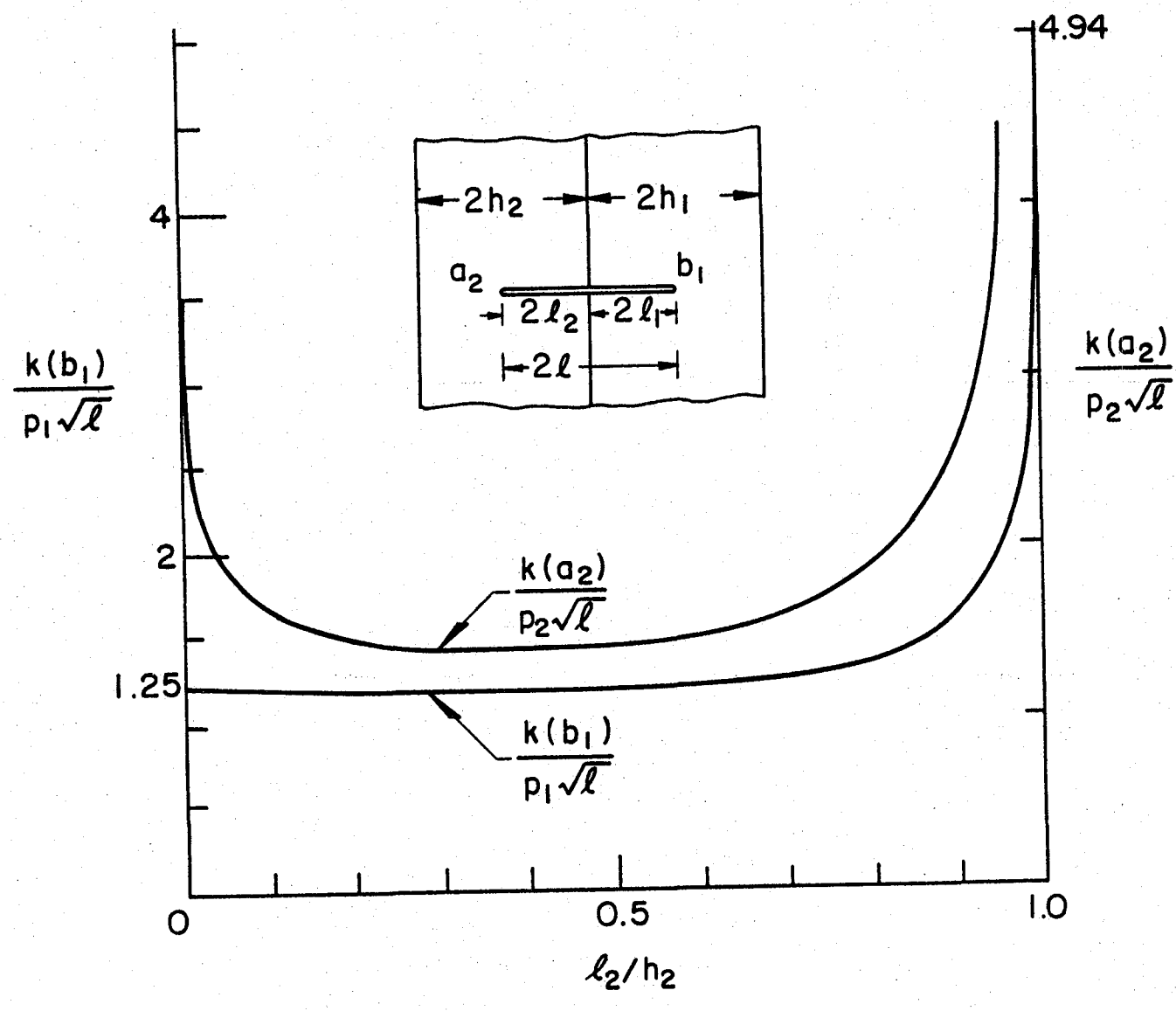

Figure 15. Stress intensity factors for an imbedded crack crossing the interface. External loads: uniform crack surface pressures p_1, p_2, $\mu_1=3\mu_2$, $\nu_1=\nu_2=0.3$, $p_1=3p_2$, $h_1=h_2$, $b_1=2\ell_1=h_1$, $k(b_1)=\lim_{x_1\to b_1}\sqrt{2(x_1-b_1)}\sigma_{1yy}(x_1,0)$, $k(a_2)=\lim_{x_2\to a_2}\sqrt{2(a_2-x_2)}\sigma_{2yy}(x_2,0)$.

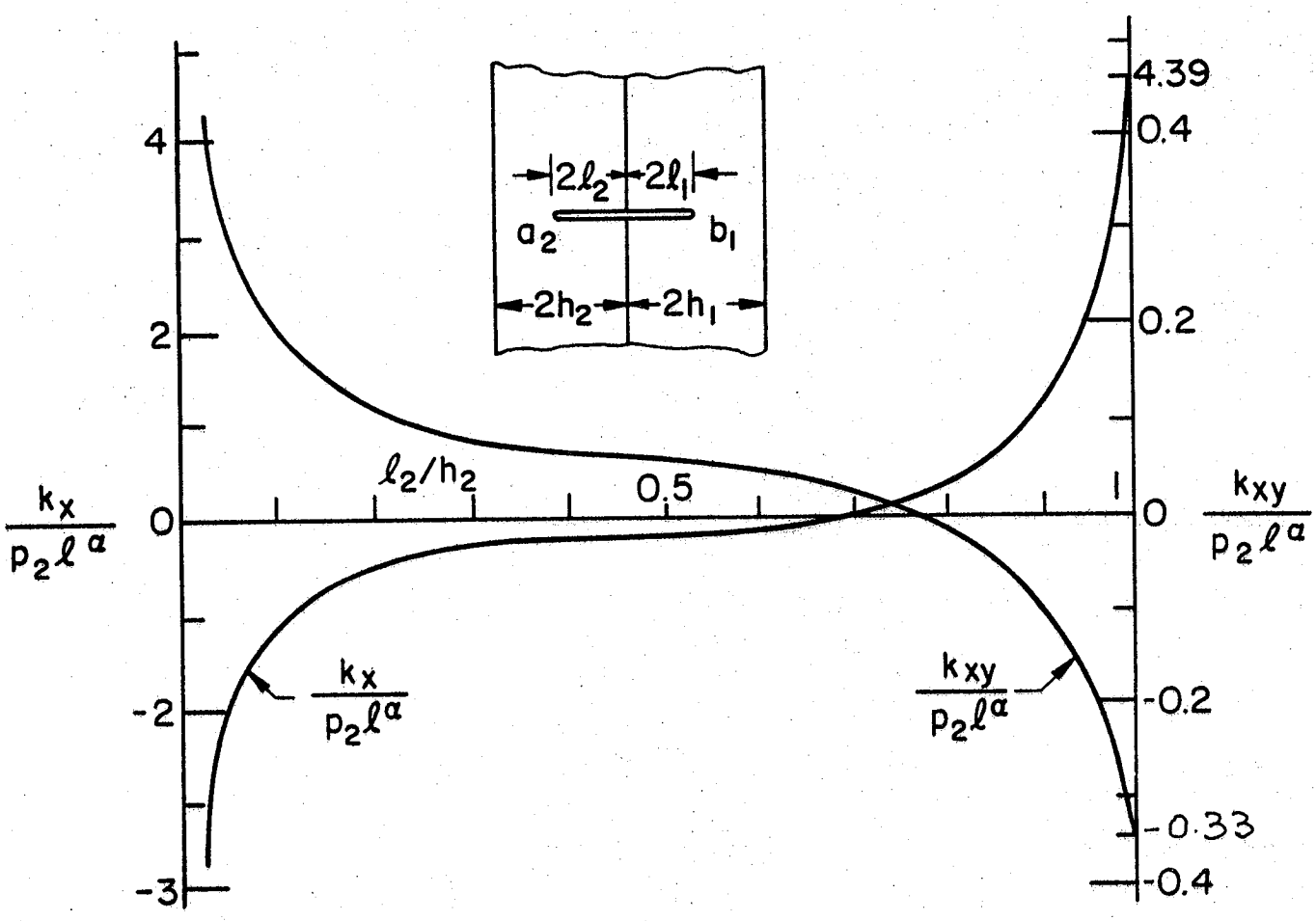

Figure 16. Same as Figure 15. $k_x = \lim_{y\to 0} y^\alpha \sigma_{xx}(0,y)$, $k_{xy} = \lim_{y\to 0} y^\alpha \sigma_{xy}(0,y)$, $\alpha = 0.079898$.

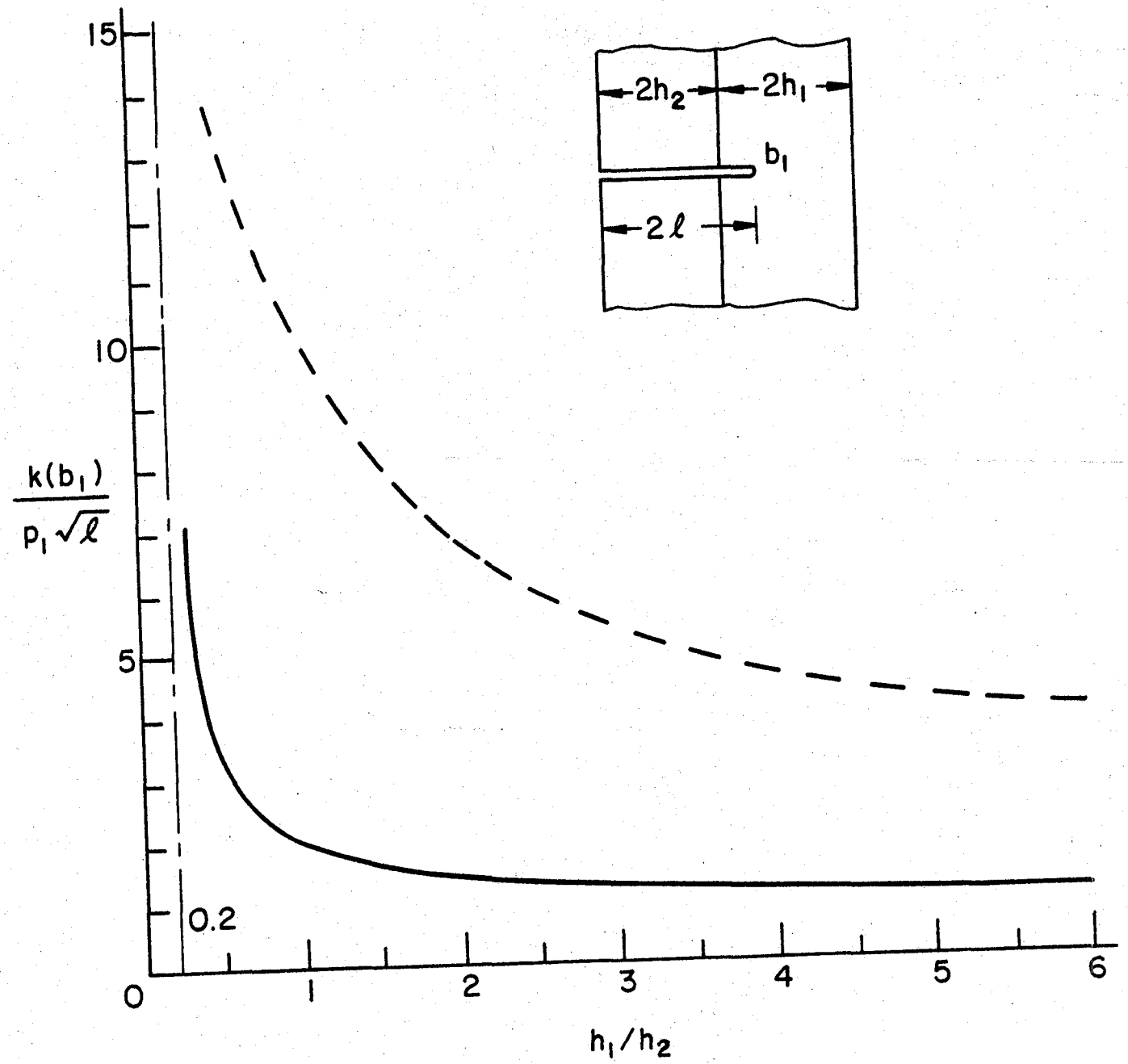

Figure 17. Stress intensity factor for an edge crack crossing the interface. $k(b_1)=\lim_{x_1\to b_1}\sqrt{2(x_1-b_1)}\sigma_{1yy}(x_1,0)$. External loads: uniform crack surface pressures, p_1, p_2, $(1-\nu_1^2)p_1/E_1=(1-\nu_2^2)p_2/E_2$, $\ell/h_2=1.2$, solid curve: $\mu_1=3\mu_2$, $\nu_1=0.3$, $\nu_2=0.25$, dashed curve: $\mu_1=\mu_2/3$, $\nu_1=0.25$, $\nu_2=0.3$.

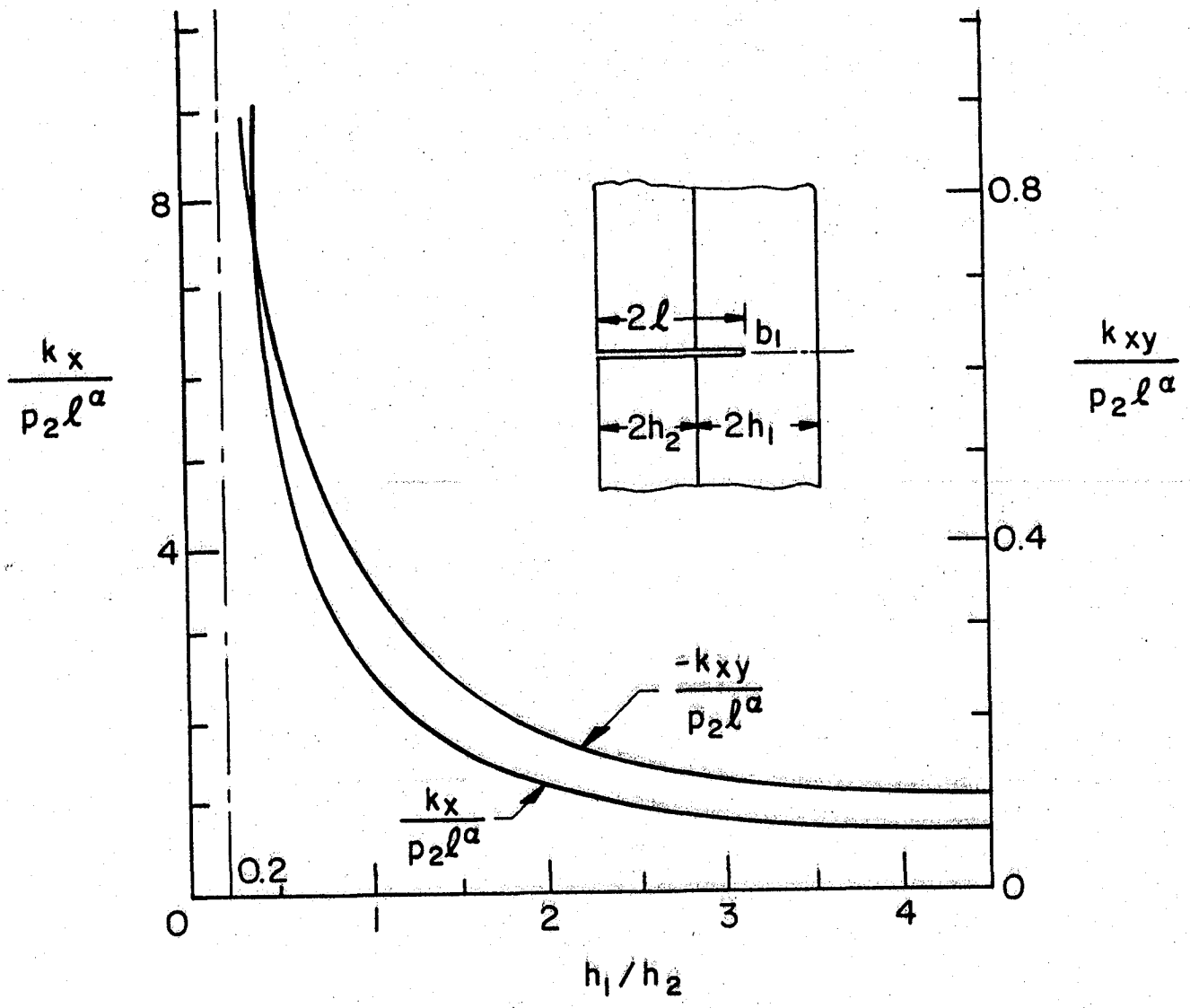

Figure 18. Stress intensity factors at the interface for an edge crack crossing the interface. $k_x = \lim_{y \to 0} y^\alpha \sigma_{xx}(0,y)$, $k_{xy} = \lim_{y \to 0} y^\alpha \sigma_{xy}(0,y)$, $\ell/h_2 = 1.2$, $\mu_1 = 3\mu_2$, $\nu_1 = 0.3$, $\nu_2 = 0.25$, $\alpha = 0.060177$.

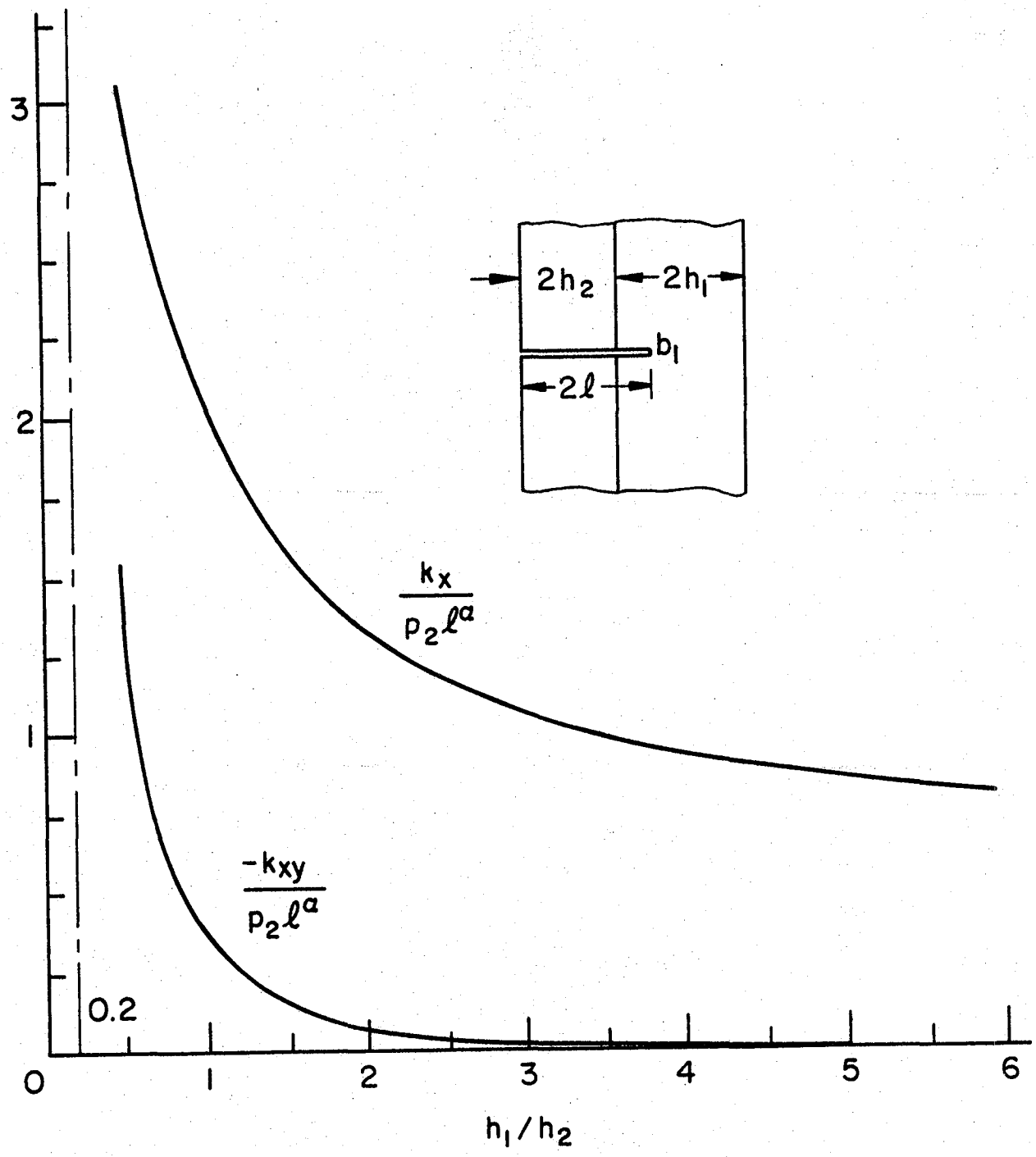

Figure 19. Same as Figure 18, $\mu_1=\mu_2/3$, $\nu_1=0.25$, $\nu_2=0.3$, $\alpha=0.060177$.

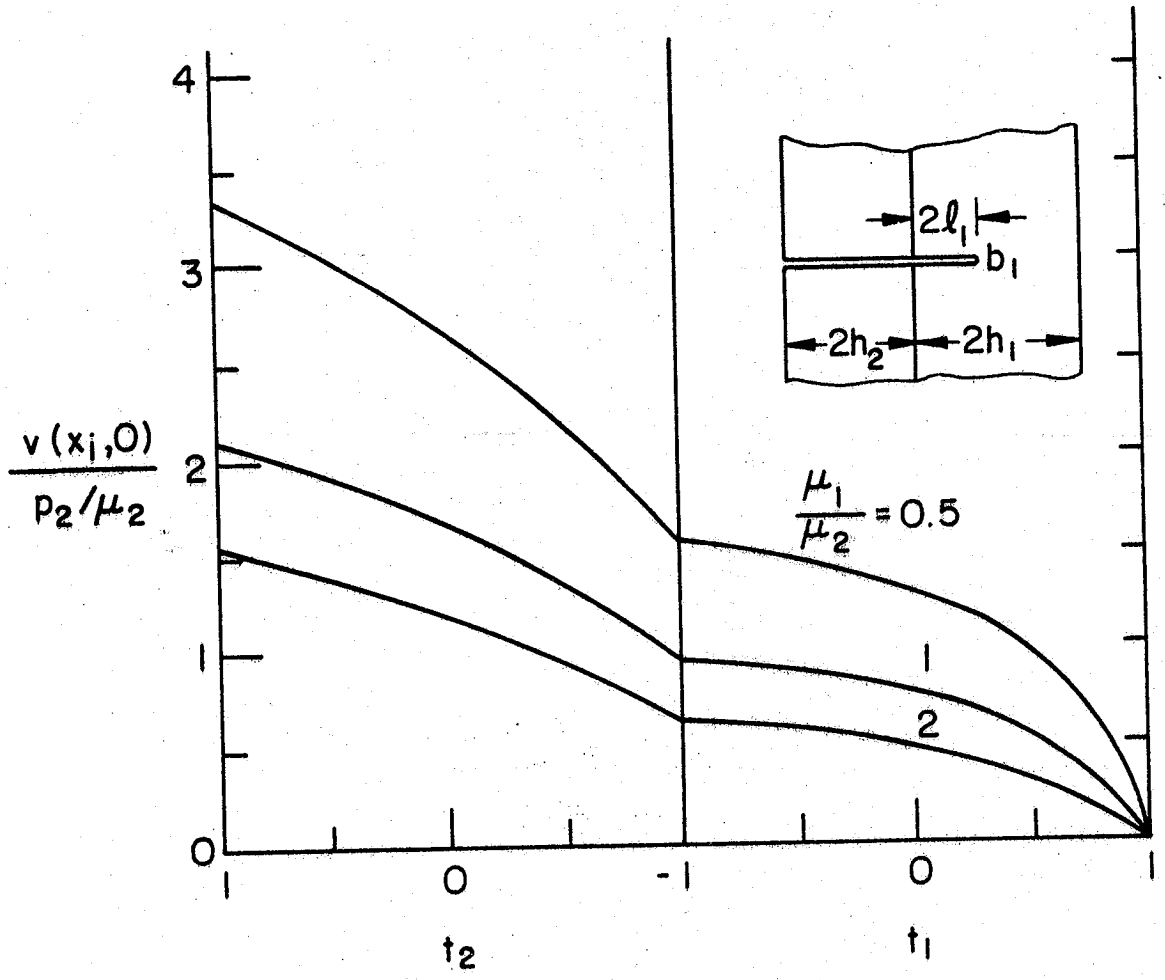

Figure 20. Crack surface displacement for an edge crack crossing the interface. Constant crack surface pressures p_1, p_2, $(1-\nu_1^2)p_1/E_1=(1-\nu_2^2)p_2/E_2$, $\nu_1=0.35$, $\nu_2=0.3$, $h_1=3h_2$, $\ell_1=0.3h_2$, $t_1=(2x_1/b_1)-1$, $t_2=1-(x_2/h_2)$.

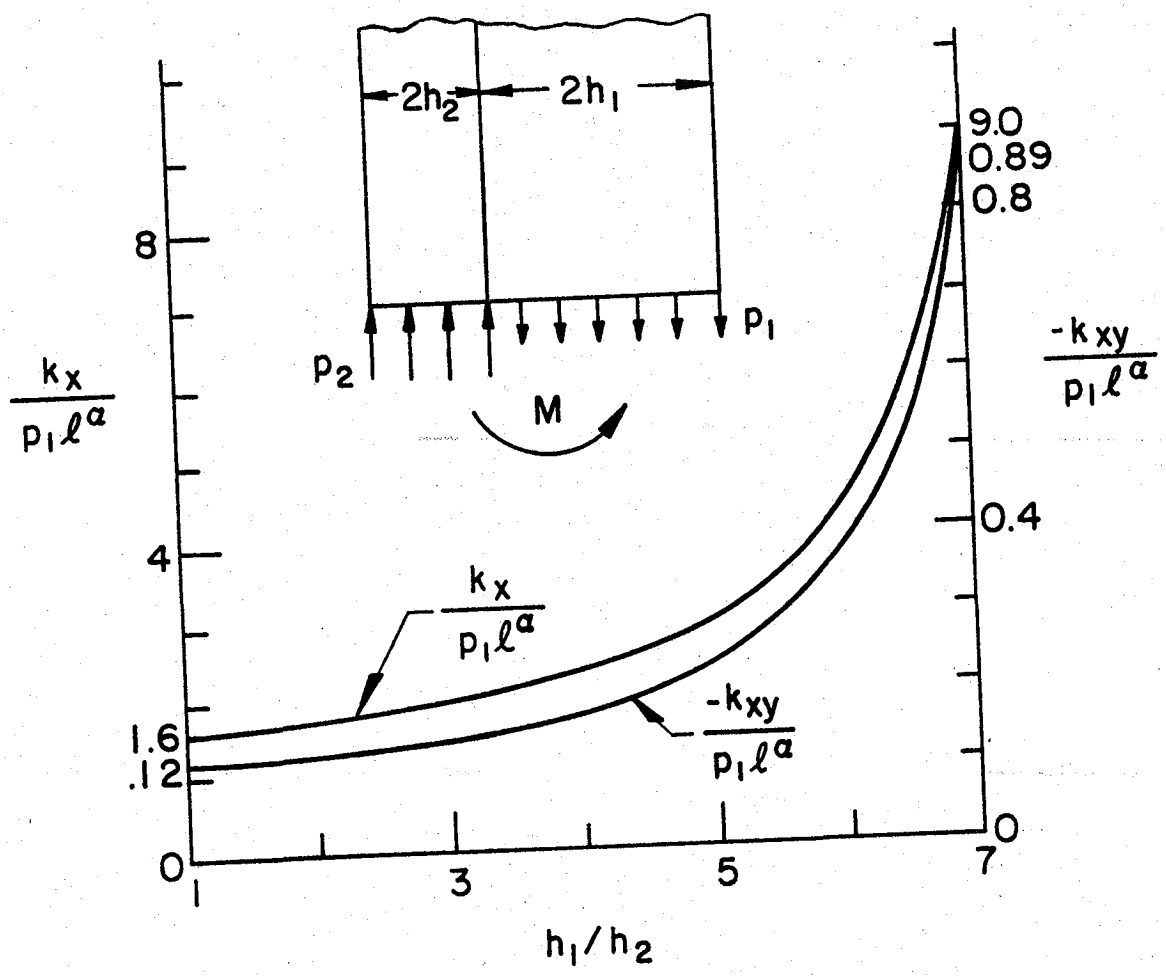

Figure 21. Stress intensity factors at the intersection of the free end and the interface in two bonded semi-infinite layers. $k_x = \lim_{y\to 0} y^{\alpha}\sigma_{xx}(0,y)$, $k_{xy} = \lim_{y\to 0} y^{\alpha}\sigma_{xy}(0,y)$, $\mu_1 = 3\mu_2$, $\nu_1 = 0.3$, $\nu_2 = 0.25$, $\alpha = 0.060177$, $p_2 = -p_1 h_1/h_2$, $\ell = h_1 + h_2$, $M = 2p_1 h_1 \ell$.

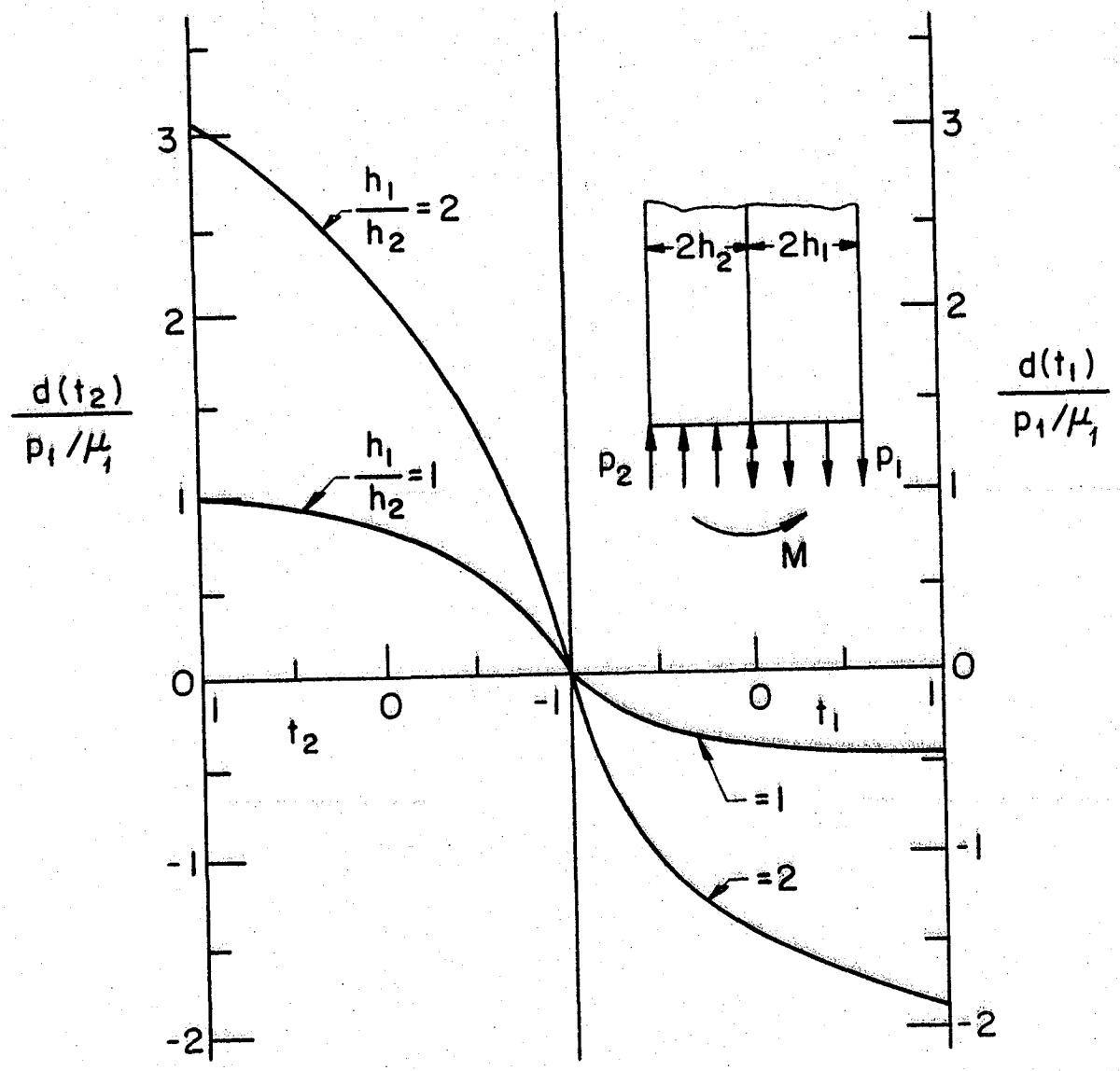

Figure 22. Relative displacement in y-direction at the free end of two bonded semi-infinite layers. $\mu_1=3\mu_2$, $\nu_1=0.3$, $\nu_2=0.25$, $t_1=(x_1/h_1)-1$, $t_2=1-(x_2/h_2)$, $d(t_i)=v_i(t_i)-v_o$, $(i=1,2)$, $v_o=v_i(0,0)$.

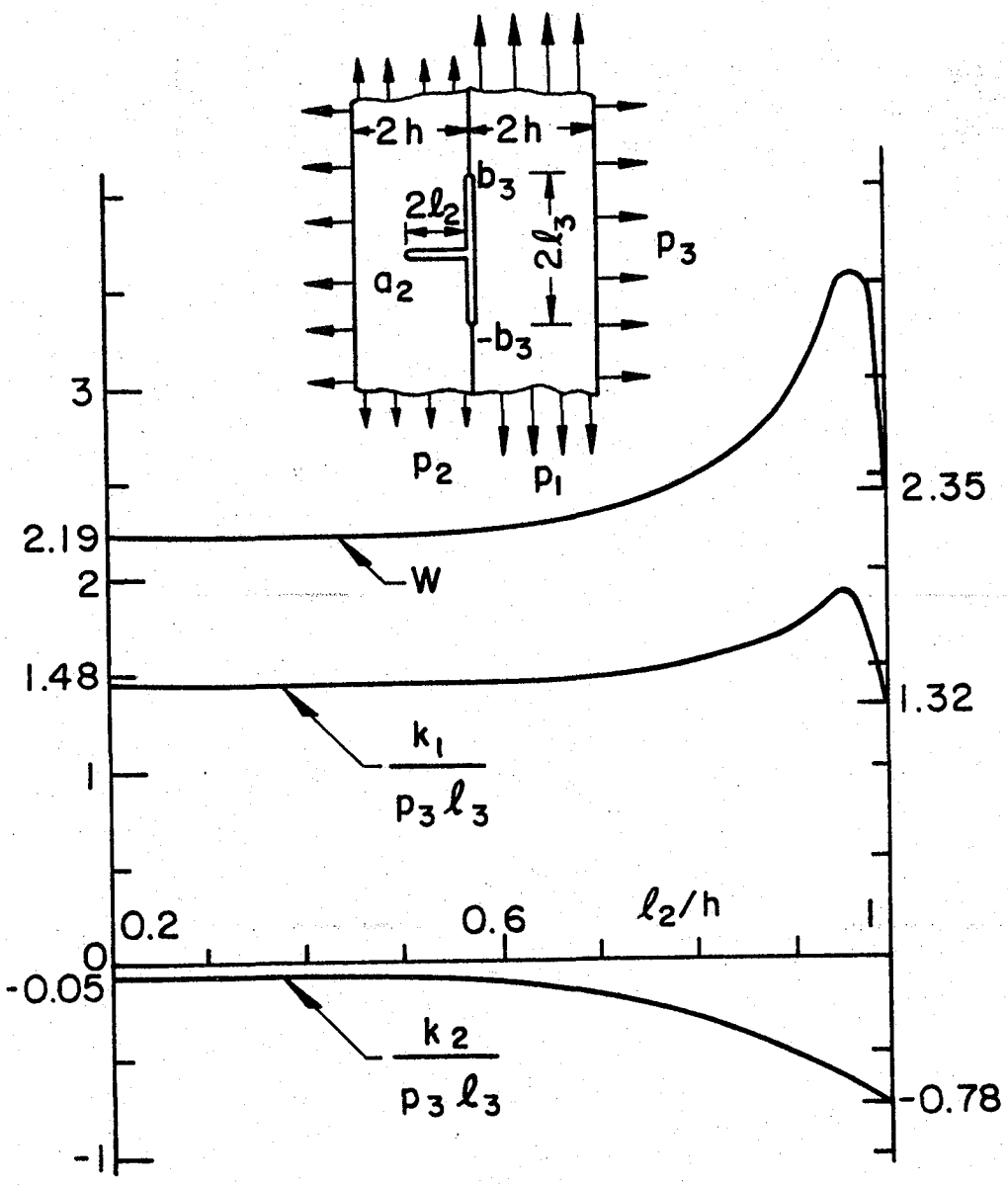

Figure 23. Stress intensity factors and the strain energy release rate, W for a uniformly pressurized T-shaped crack. $p_3=p_2$, $p_4=0$, $h_1=h_2=h$, $b_3=\ell_3=h$, $\mu_1=3\mu_2$, $\nu_1=\nu_2=0.3$, $k_1+ik_2=\lim_{y\to b_3}(b_3-y)^{\beta_3}(b_3+y)^{\alpha_3}[\sigma_{1xx}(0,y)+i\sigma_{1xy}(0,y)]$, $W=(k_1^2+k_2^2)/p_3^2\ell_3^2$.

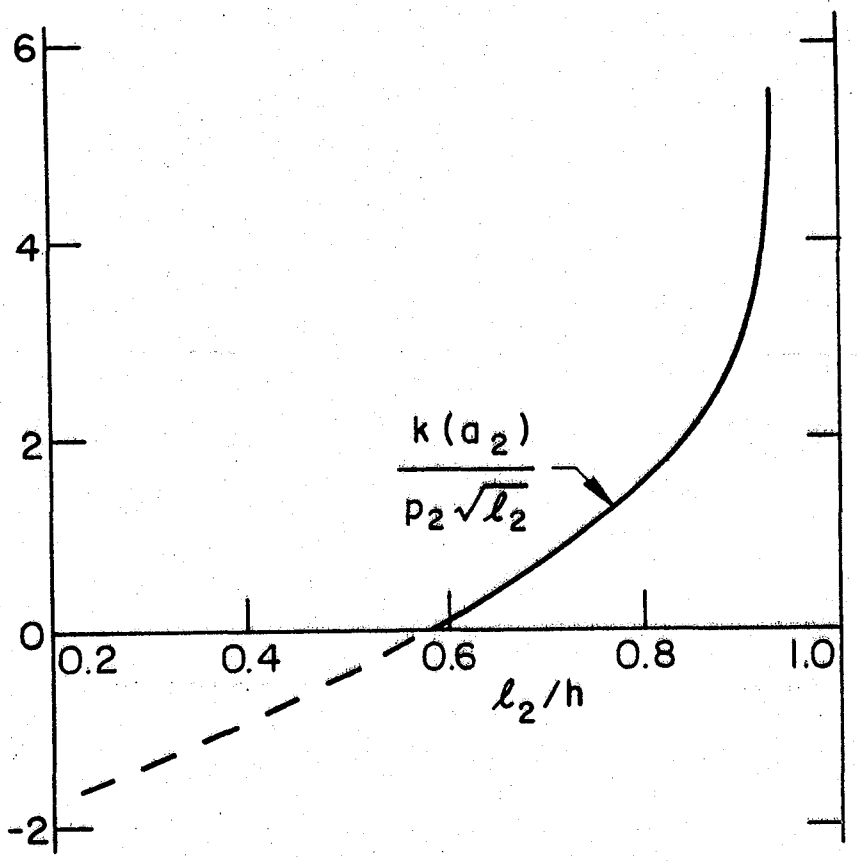

Figure 24. Stress intensity factor $k(a_2)$ for an internally pressurized T-shaped crack (data same as in Figure 23).

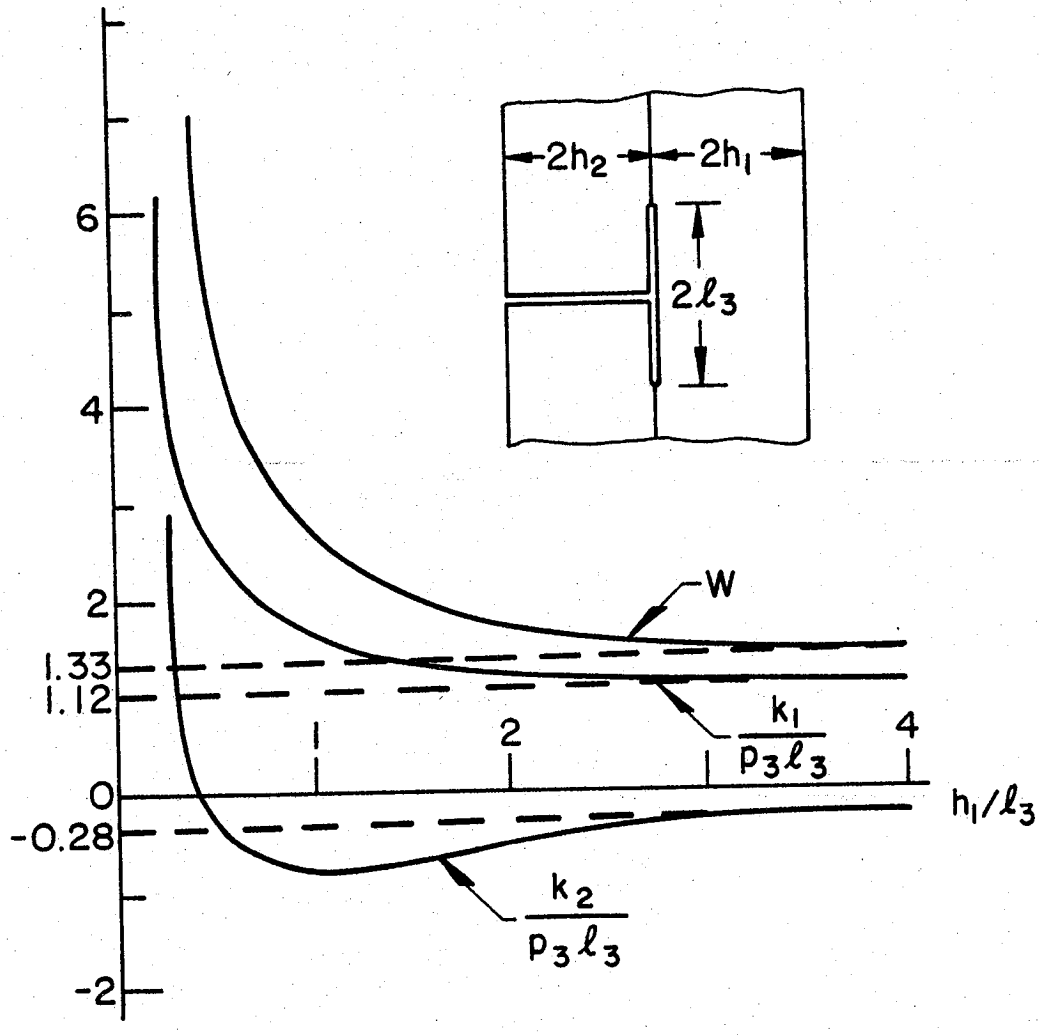

Figure 25. Stress intensity factors and the strain energy release rate W for a uniformly pressurized T-shaped crack - the case of broken layer. $p_3=p_2$, $p_4=0$, $\mu_1=3\mu_2$, $\nu_1=\nu_2=0.3$, $\ell_3=h_2$.

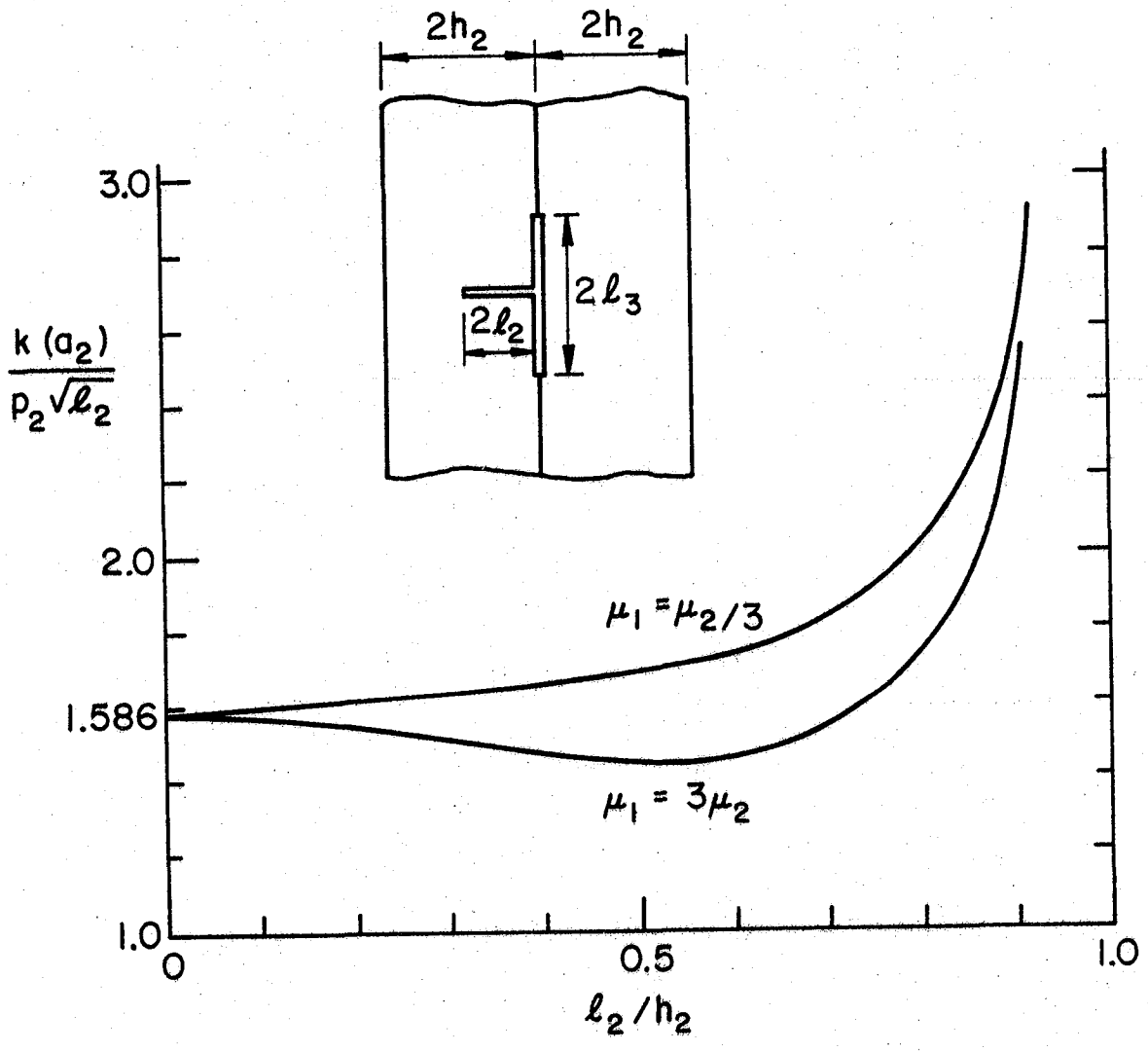

Figure 26. Stress intensity factor $k(a_2)$ for an internal T-shaped crack. $p_3=p_4=0$, $\nu_1=\nu_2=0.3$, $\ell_3=h_1=h_2$.

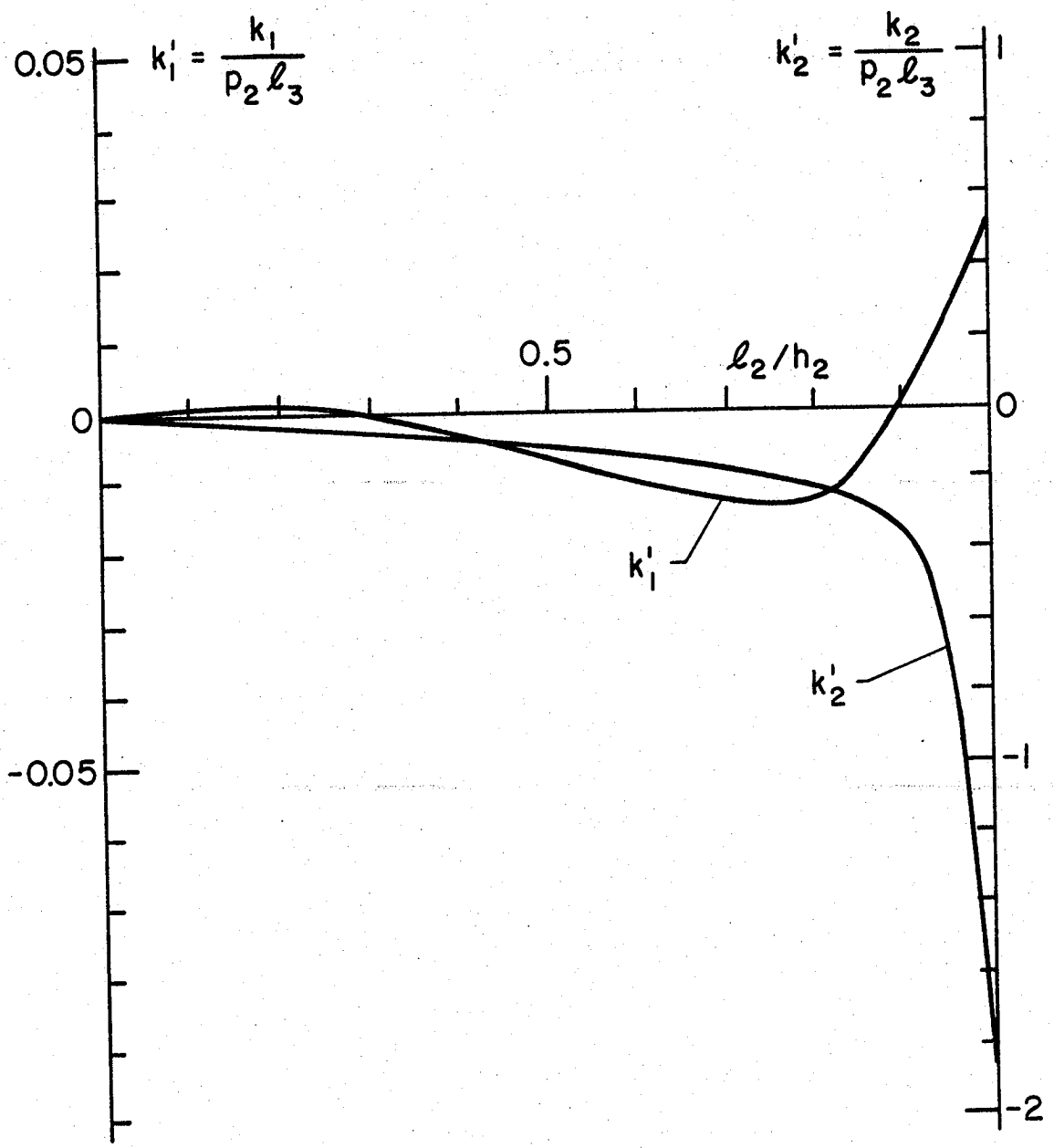

Figure 27. Stress intensity factors for the interface crack in bonded layers containing a T-shaped crack. $p_3=p_4=0$, $\mu_1=\mu_2/3$, $\nu_1=\nu_2=0.3$, $\ell_3=h_1=h_2$ (see insert in Figure 26).

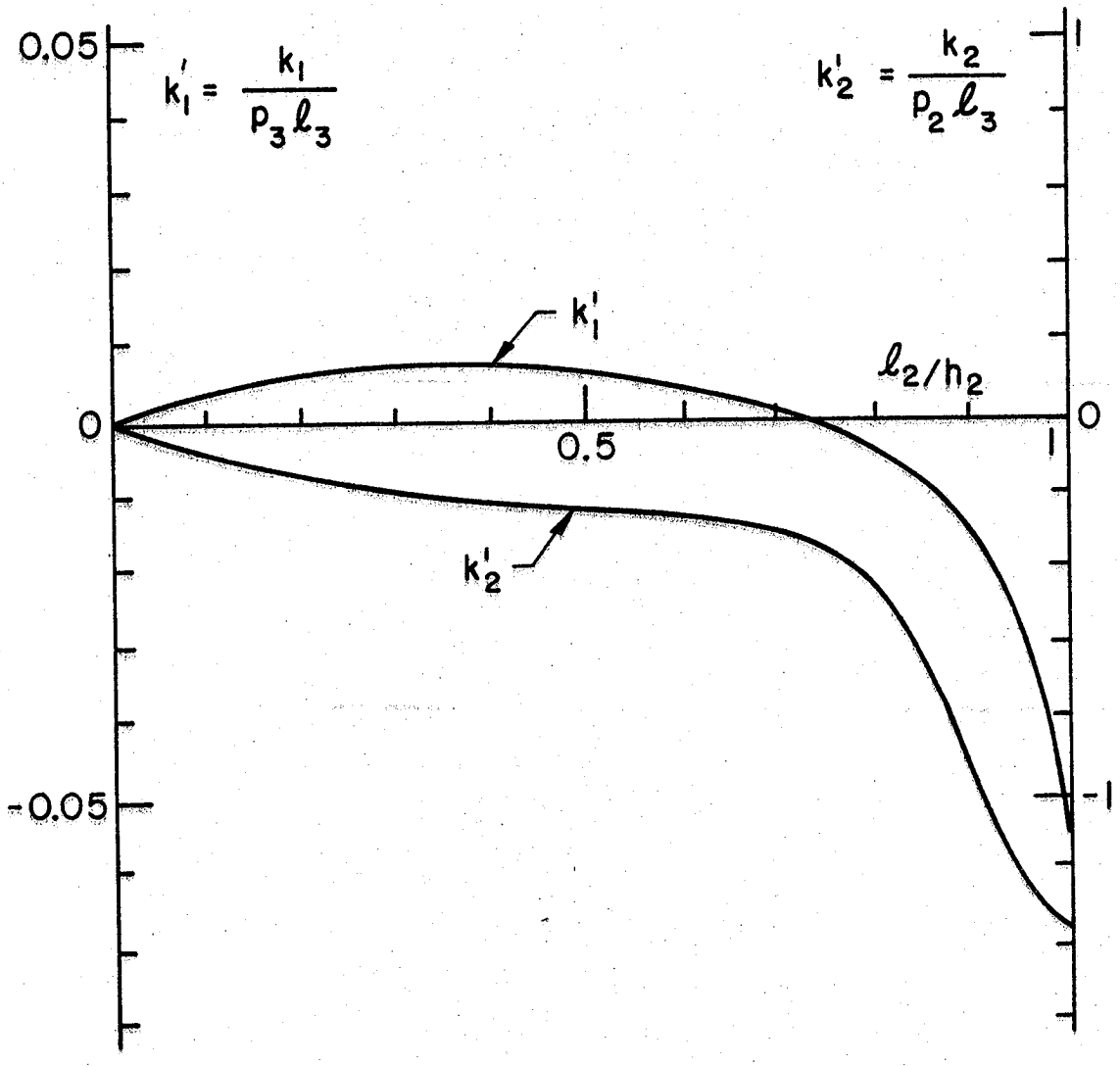

Figure 28. Same as Figure 27. $\mu_1 = 3\mu_2$, $\nu_1 = \nu_2 = 0.3$.

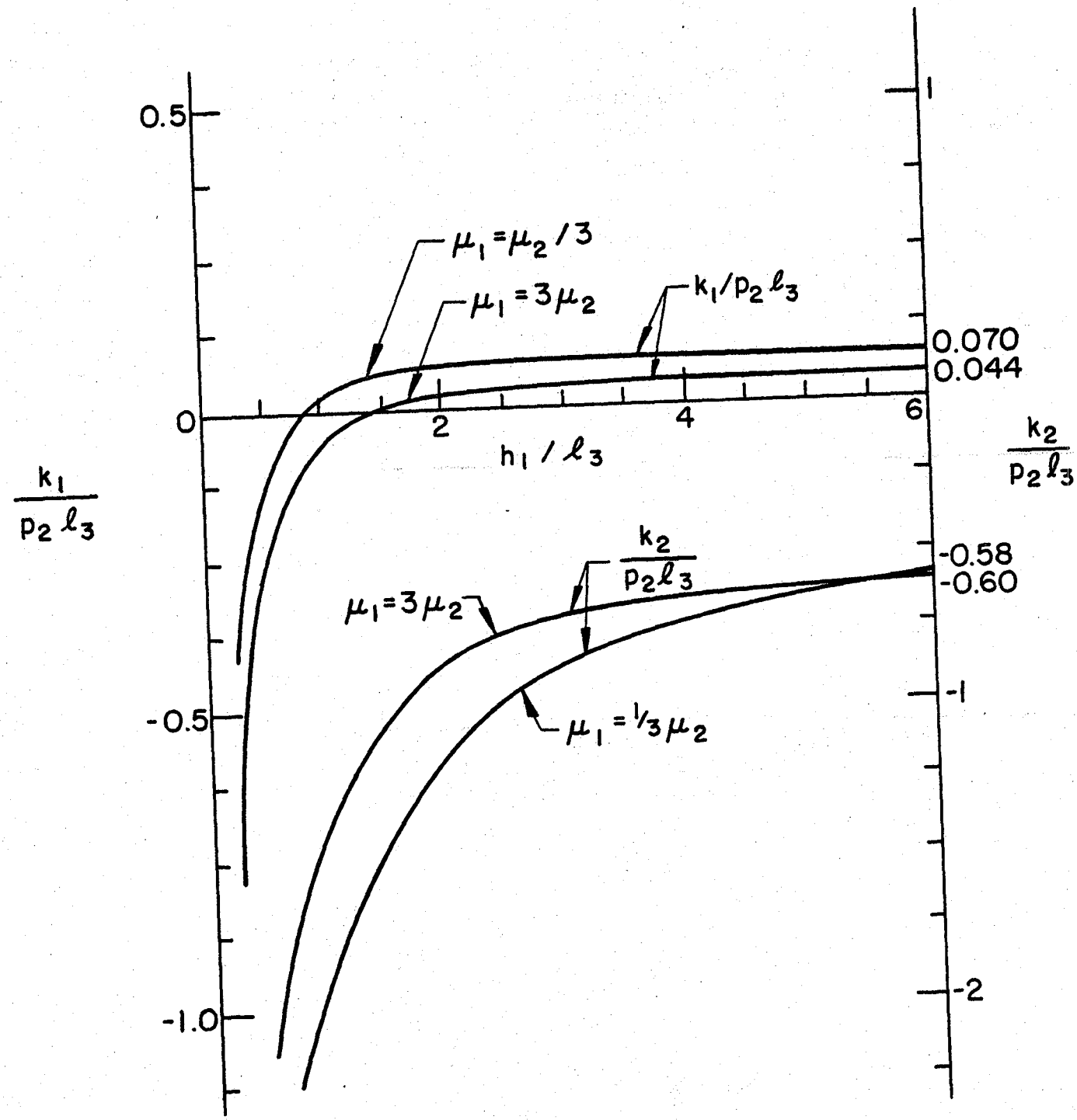

Figure 29. Stress intensity factors at the interface crack tip in bonded layers containing a T-shaped crack - the case of broken layer. $\nu_1=\nu_2=0.3$, $\ell_3=h_2$.

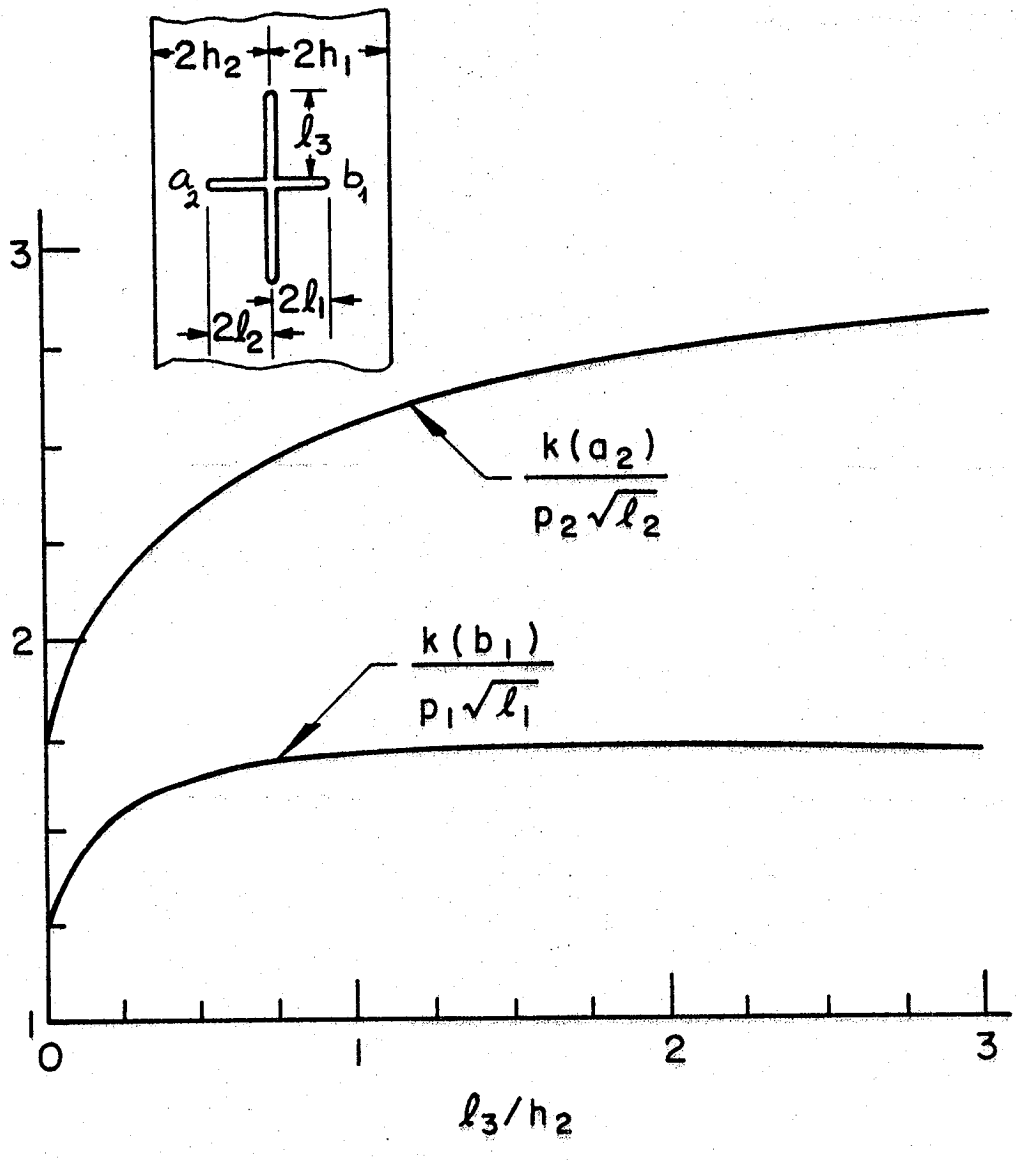

Figure 30. Stress intensity factors $k(a_2)$ and $k(b_1)$ for a symmetric cross-shaped crack in bonded layers loaded in tension away from the crack region. $\mu_1=3\mu_2$, $\nu_1=\nu_2=0.3$, $p_1=3p_2$, $p_3=p_4=0$, $h_1=h_2=2\ell_1=2\ell_2$.

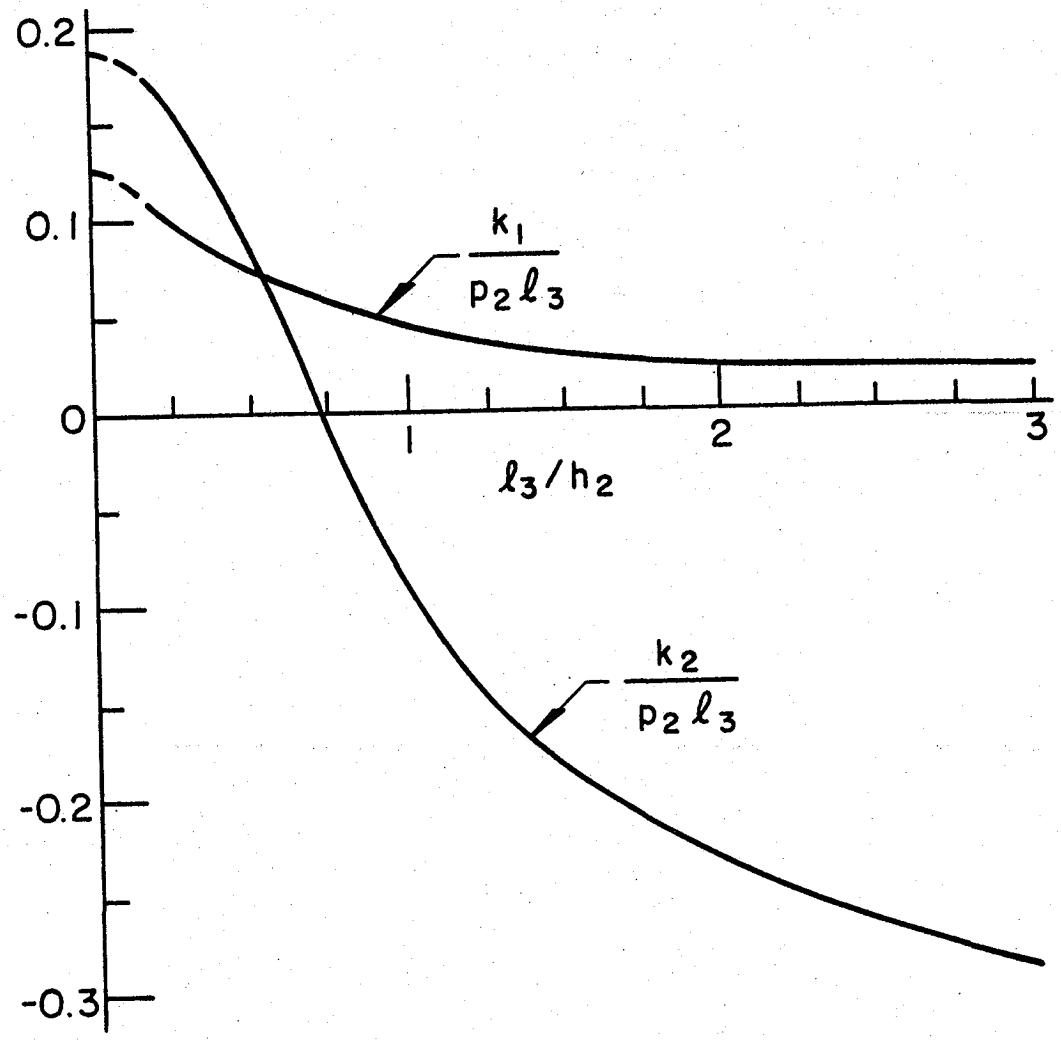

Figure 31. Stress intensity factors for the interface crack in bonded layers containing a symmetric cross-shaped crack (data same as in Figure 30).

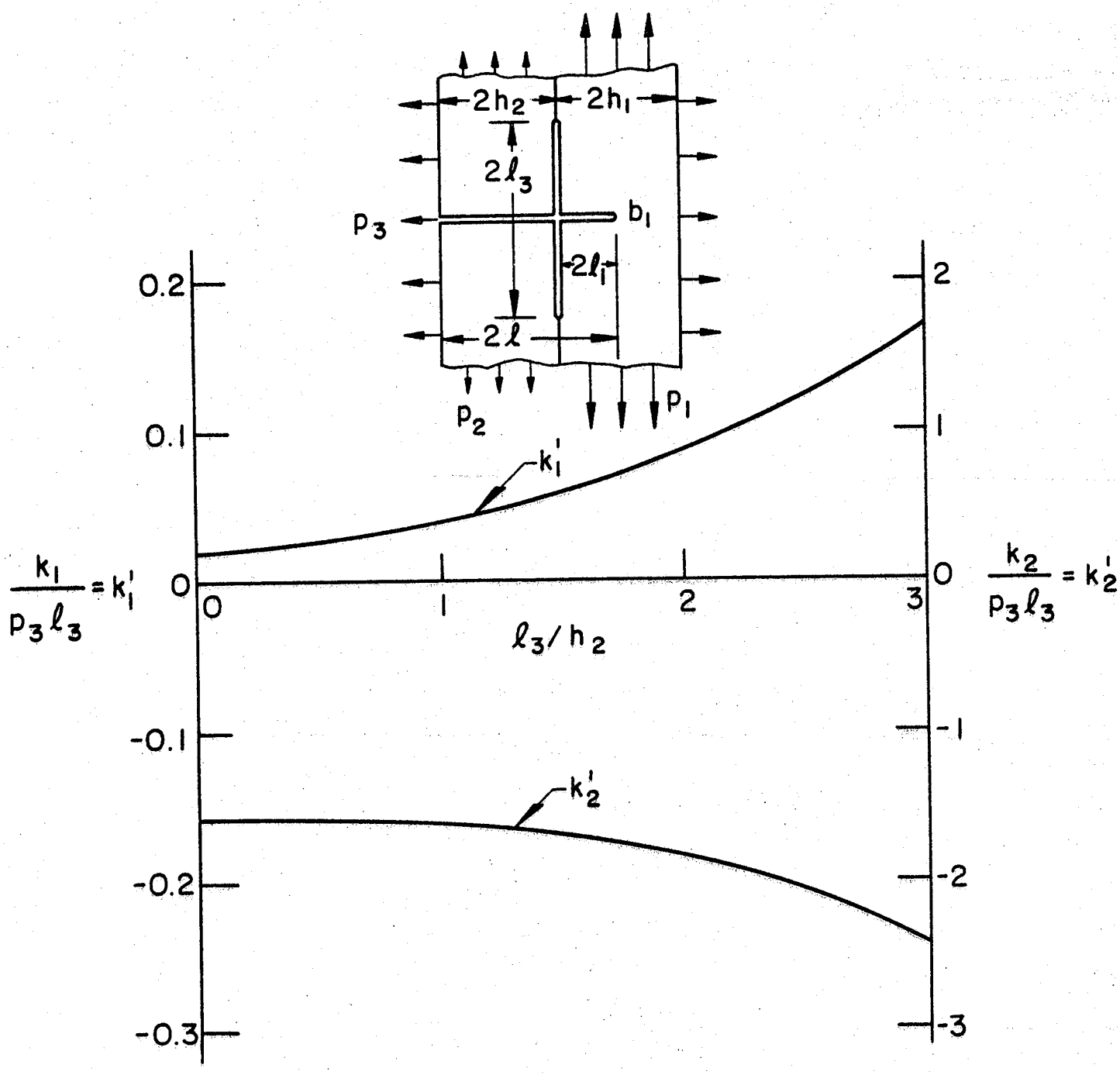

Figure 32. Stress intensity factors for the interface crack in bonded layers containing an internally pressurized cross-shaped crack - the case of broken layer. $\mu_1=3\mu_2$, $\nu_1=\nu_2=0.3$, $\ell_1=h_1/2$, $h_1=h_2$, $p_3=p_2$, $p_1=3.857\ p_2$, $p_4=0$.

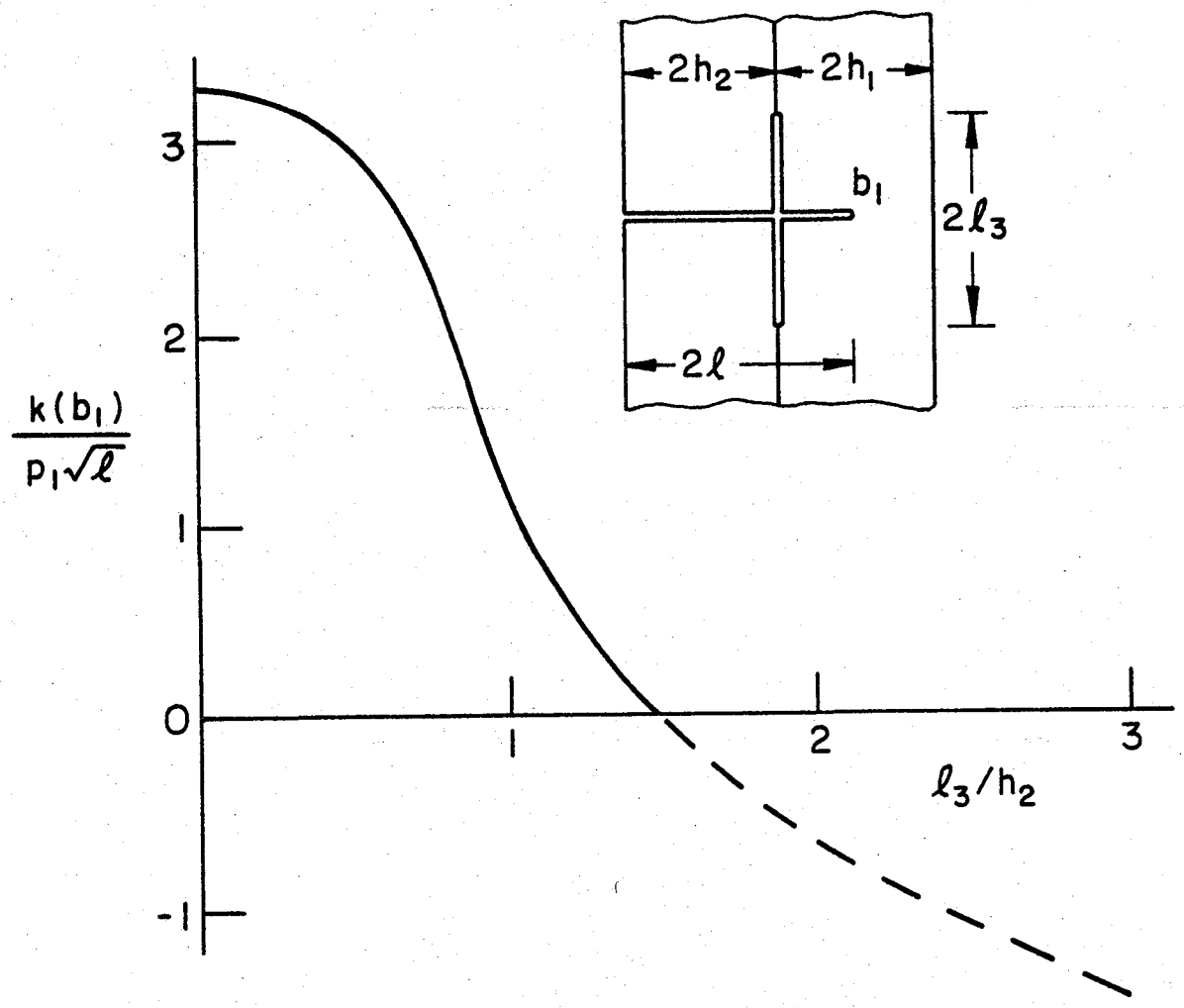

Figure 33. Same as in Figure 32, stress intensity factor at b_1.

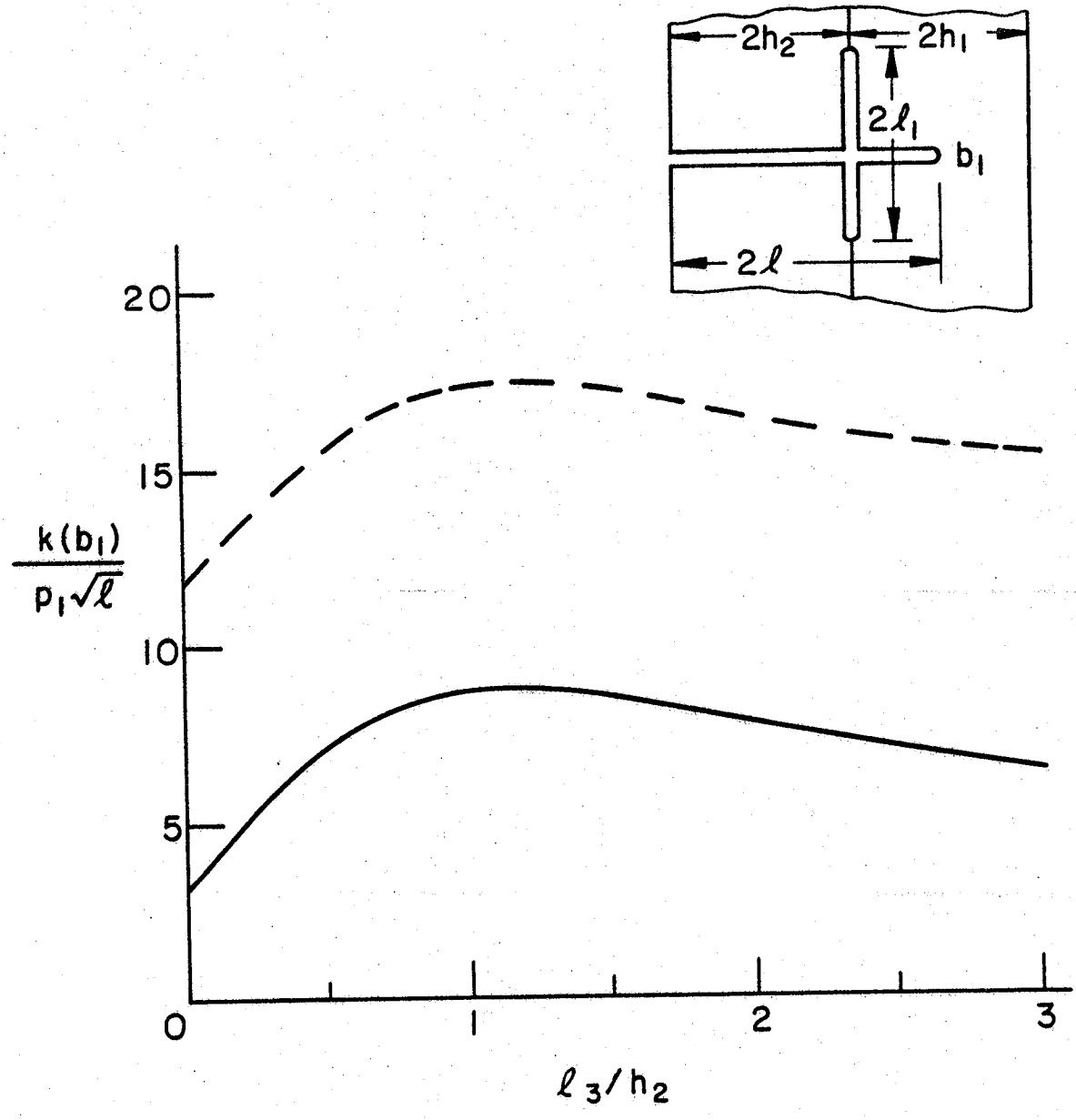

Figure 34. Stress intensity factor $k(b_1)$ in bonded layers containing a cross-shaped crack with a broken layer and loaded in tension in y direction away from the crack region, $h_1=h_2=2\ell/3$, $\nu_1=\nu_2=0.3$, $p_3=p_4=0$, solid line: $\mu_1=3\mu_2$, $p_1=3\mu_2$, dashed line: $\mu_1=\mu_2/3$, $p_1=p_2/3$.

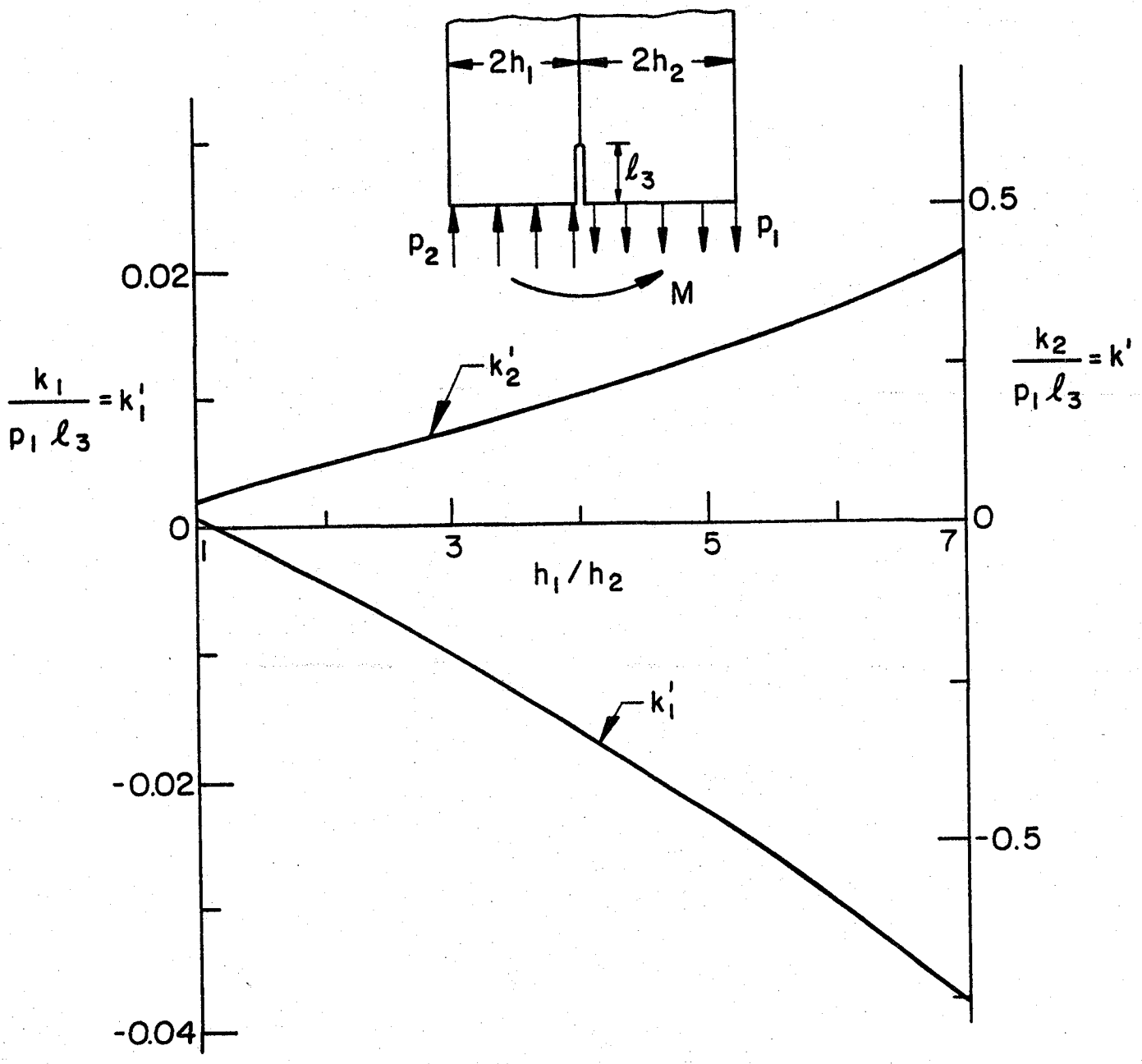

Figure 35. Stress intensity factors in a bonded semi-infinite plate with an edge crack on the interface. $\mu_1=3\mu_2$, $\nu_1=\nu_2=0.3$, $\ell_3=h_2$, $p_2h_2=-p_1h_1$, $M=2p_1h_1(h_1+h_2)$.

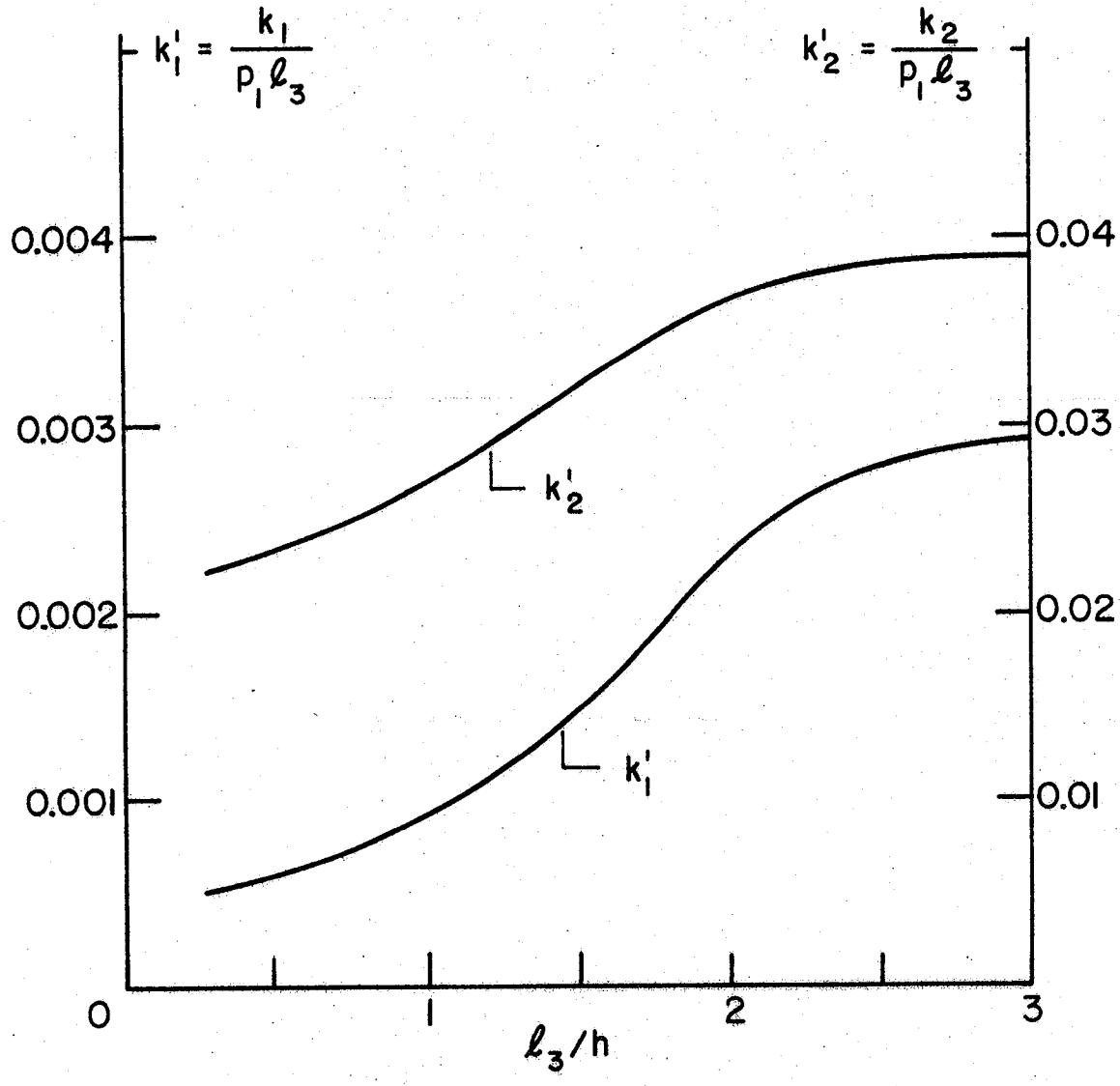

Figure 36. Stress intensity factors in a bonded semi-infinite plate with an edge crack on the interface. $\mu_1=3\mu_2$, $\nu_1=\nu_2=0.3$, $h_1=h_2=h$, $p_1=p_2$, $M=4p_1h^2$.